ELSEVIER

Journal of Structural Geology 30 (2008) 237–256

JOURNAL OF STRUCTURAL GEOLOGY

www.elsevier.com/locate/jsg

Fault zone architecture and permeability features in siliceous sedimentary rocks: Insights from the Rapolano geothermal area (Northern Apennines, Italy)

Andrea Brogi*

Dipartimento di Scienze della Terra, Università di Siena, Via Laterina, 8, 53100 Siena, Italy

Received 31 October 2006; received in revised form 8 October 2007; accepted 17 October 2007
Available online 12 November 2007

Abstract

Studies of fracture networks and hydrothermal mineralisation of several faults affecting Jurassic siliceous sedimentary rocks, exposed in the Rapolano geothermal area (hinterland of the Northern Apennines, Italy), allow us to characterise the fault zone architectures and their permeability features. The study structures are normal faults with displacements of anything up to 30–40 m, belonging to a fossil hydrothermal system, Pleistocene in age. The fault zones are characterised by asymmetrical damage zones which are thickest in the hangingwall blocks. Fracture networks mainly consist of a subvertical fracture set at about 45° with respect to the fault plane. Widespread hydrothermal alteration (illite/smectite and kaolinite) and mineralisation consisting of quartz, calcite, dolomite, malachite, azurite and iron oxides characterise the fractures of the damaged rocks. This mineralisation suggests the occurrence of extraformational fluid circulation during the latest stage of faulting. Fault cores are characterised by cemented fault rock up to 25 cm thick, consisting of protocataclasite and ultracataclasite layers, grading to crush and fine crush breccia strongly affected by minor C_1-type shear planes. Fault cores represented barriers to fluid flow during the latest stage of faulting, whereas they acted as conduits during the initial stages. Fault zones with similar features are presently affected by hydrothermal circulation (thermal water up to 39 °C, and CO_2). The hydrothermal fluids give rise to several thermal springs and are exploited at depth for thermal resorts and CO_2 extraction, both in the Rapolano area and surroundings. A similar scenario characterises the Larderello-Travale and Mt. Amiata geothermal areas, where hydrothermal fluids and steam are industrially exploited for electricity production. The main results of this study are that the damage zone is asymmetrical and widest in the hangingwall. This could represent a useful contribution to the prediction of hydrothermal fluid pathways and geothermal targets in all the geothermal areas with similar features to those described here.
© 2007 Elsevier Ltd. All rights reserved.

Keywords: Fault zone architecture; Permeability; Fractures; Siliceous rocks; Geothermal areas

1. Introduction

Studies on fault zone architecture represent the main means for reconstructing or predicting the fluid flow pattern in the shallow Earth's crust. The faults are brittle structures often accompanied by a complex fracture network, providing permeable pathways for fluids from the surface down to deeper crustal levels (Billi et al., 2007), and vice versa, as is occurring in geothermal areas where fault zones are important conduits for large-volume flow of exploitable hydrothermal fluids and steam (Barbier, 2002; Bellani et al., 2004). For this reason, active or inactive faults occurring in those areas characterised by anomalous heat-flow are considered of strategic interest for geothermal (low- or high-enthalpy) and ore deposit exploration, respectively. It has been documented that several fault zones can act either as a barrier or, in contrast, conduits for fluid circulation (Caine et al., 1996; Aydin, 2000; Jourde et al., 2002). Laboratory experiments and numerical simulation demonstrated that the permeability of a fault zone is anisotropic, and at its maximum if the fluid flow is parallel to the fault plane (Sibson, 1996; Evans et al., 1997; Caine and Forster, 1999; Jourde et al., 2002). Fault-parallel permeability

* Tel.: +39 0577 233972; fax: +39 0577 233938.
E-mail address: brogiandrea@unisi.it

0191-8141/$ - see front matter © 2007 Elsevier Ltd. All rights reserved.
doi:10.1016/j.jsg.2007.10.004

can be enhanced by nearly an order of magnitude relative to the host rock; by contrast, fault-normal permeability may be two orders of magnitude less then the host rock. In this view, the three-dimensional nature of the fracture network characterising the fault zones is a primary factor controlling the fault-related permeability (Bruhn et al., 1990; Evans et al., 1997; Caine and Forster, 1999). Conduits, barriers or combined conduit-barriers in hydrological systems of fault zones strictly depend on the fault architecture resulting from a complex set of components, such as the fault core and the damage zone (Chester and Logan, 1986; Chester et al., 1993; Caine et al., 1996; Cello et al., 2001a,b). Studies on fault zones and fluid flow have been carried out in several parts around the world, in different geological contexts, for understanding both the fluid flow pattern and the seismological response (Parry and Bruhn, 1986; Blampied et al., 1992; Sibson, 1992, 1996; Byerlee, 1993; Barton et al., 1995). A large number of studies considered active or inactive fault zones, developed in metamorphic (Wibberley and Shimamoto, 2003; Rowland and Sibson, 2004), magmatic (Parry et al., 1988, 1991; Bruhn et al., 1994; Evans and Chester, 1995; Barton et al., 1995) and sedimentary rocks such as sandstones (Antonellini and Aydin, 1994, 1995; Nelson et al., 1999; Flodin and Aydin, 2004) or carbonates (Cello, 2000; Cello et al., 2000, 2001a,b; Peacock, 2001; Storti et al., 2003; Labaume et al., 2004; Kim et al., 2004; Agosta and Aydin, 2006; Micarelli et al., 2006; Billi et al., 2007). Nevertheless, very scarce data have been published for siliceous sedimentary rocks, such as the radiolarites. These rocks, broadly exposed in the hinterland of the Northern Apennines, consist of the very thick (up to 150 m) stratigraphic succession, Jurassic in age, of the Tuscan Nappe sedimentary tectonic unit. These rocks represent an important succession for geothermal exploitation because, together with the Jurassic carbonates, they give rise to the shallowest geothermal reservoir drilled at depth in the Larderello-Travale and Mt. Amiata geothermal areas (Batini et al., 2003 and references therein) (Fig. 1). In addition, several thermal springs and gas vents occurring in southern Tuscany are strictly related to fault zones developed within the Jurassic radiolarites.

In order to detail the characteristics of the fault zones, the nature of the hydrothermal alteration and the permeability structure within the Jurassic radiolarites, the fault zones of several Pleistocene normal faults, which acted as conduits for hydrothermal circulation, have been analysed in the Rapolano geothermal area. This area is characterised by widespread hydrothermal circulation (low-enthalpy geothermal resources) active from the Pleistocene. Hydrothermal circulation gave rise to broad Pleistocene–Holocene travertine deposits (Barazzuoli et al., 1988; Guo and Riding, 1992, 1994, 1996;

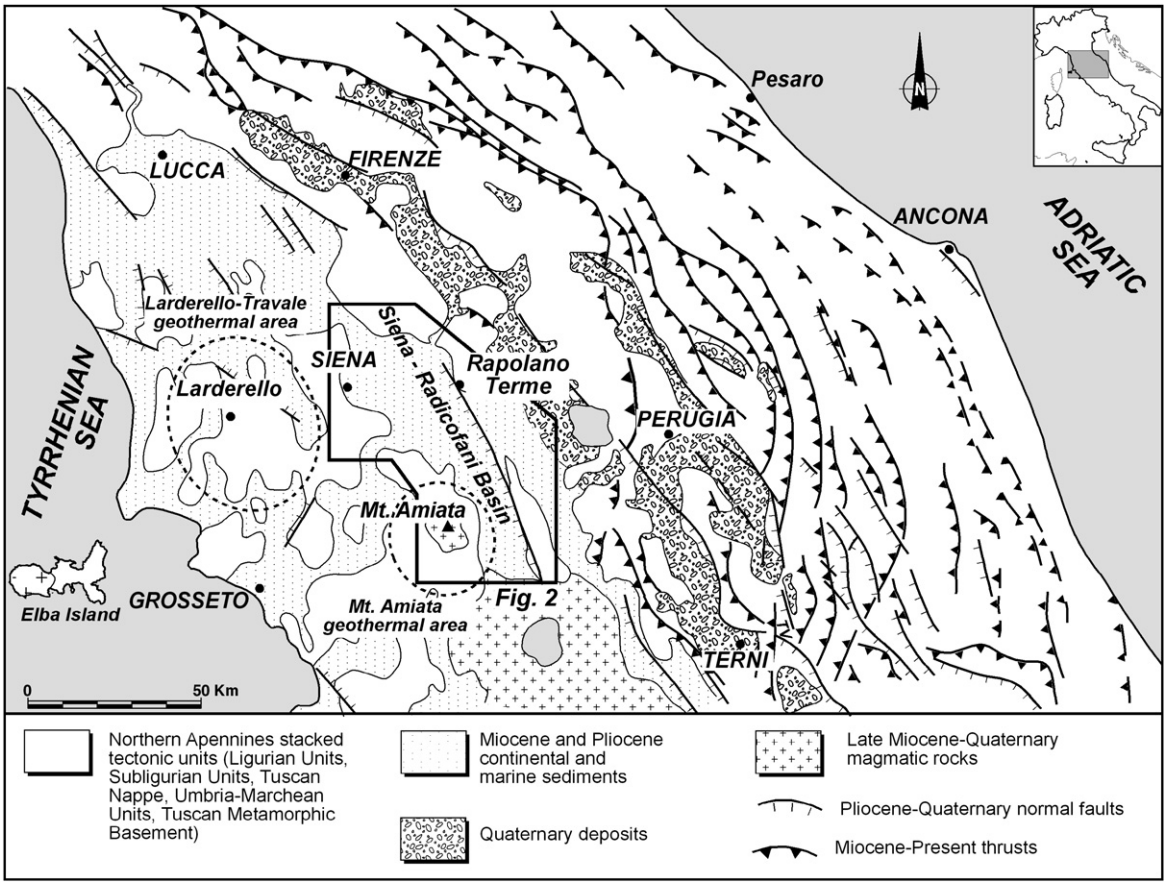

Fig. 1. Geological sketch map of the Northern Apennines and its geological evolution (from Liotta et al., 1998, modified). The location of the study area, enlarged in Fig. 2, is also indicated.

Brogi et al., 2002) and presently causes geothermal springs of up to 39 °C, and CO_2 leakage (Minissale et al., 2002).

2. Geological setting

The Rapolano geothermal area is located in the eastern side of the Siena Basin (Costantini et al., 1982; Martini and Sagri, 1993), a tectonic depression developed during the Neogene extensional collapse of the hinterland of the Northern Apennines (Bertini et al., 1991; Carmignani et al., 1994) (Fig. 1). The Siena Basin represents the central part of a broad tectonic depression about 90 km long and NNW–SSE oriented, known as the Siena-Radicofani Basin (Bossio et al., 1993 with references therein) (Fig. 2). The northern part of this tectonic depression, named the Casino Basin, was mainly filled by Late Miocene continental to brackish sediments (Lazzarotto and Sandrelli, 1977). The southern part (the Radicofani Basin) consists of Early–Middle Pliocene marine sediments (Bossio et al., 1993; Liotta, 1994, 1996; Liotta and Salvatorini, 1994), whereas Middle–Late Miocene deposits were encountered at depth by boreholes (Bossio et al., 1993; Liotta, 1996). In the central part (the Siena Basin), Early–Middle Pliocene and Quaternary deposits are broadly exposed (Costantini et al., 1982; Gandin, 1982; Gandin and Sandrelli, 1992). Pliocene sediments mainly consist of marine clays, marly-clays, sands, gravels and conglomerates. The Quaternary sediments are composed of continental gravels, sands with interbedded clays, and travertines.

The Siena Basin is characterised by high heat flow, locally reaching 140 mW/m^2 (Mongelli et al., 1982), coinciding with the average value for southern Tuscany (Della Vedova et al., 2001), except for the Larderello-Travale and Mt. Amiata geothermal areas where heat flow values reach up to 1000 mW/m^2 and 600 mW/m^2, respectively (Della Vedova et al., 2001; Batini et al., 2003 and references therein). In the Siena Basin the temperature increasing with depth has been locally evaluated to be 55–60 °C/km as deduced by direct measurement within boreholes (Mongelli et al., 1982) (Fig. 2).

The eastern margin of the Siena Basin is bounded by a west-dipping, NNW–SSE striking normal fault known as the Rapolano Fault (Costantini et al., 1982; Bertini et al., 1991; Bonini and Sani, 2002; Brogi et al., 2002) (Fig. 2). This fault corresponds to the northern prolongation of the fault system delimiting the eastern margin of the Radicofani Basin, described for the Mt. Cetona area (Passerini, 1964; Liotta and Salvatorini, 1994; Liotta, 1996). The Rapolano Fault has been mapped at the surface for about 10 km from Rapolano to Trequanda, marking the eastern structural and physiographical boundary of the Siena Basin (Fig. 2). The Rapolano Fault separates, in several places, Neogene sediments from pre-Neogene rocks exposed in the Rapolano-Trequanda Ridge (Fig. 3), part of the Mts. Chianti–Mt. Cetona morphotectonic feature where pre-Neogene carbonate and turbiditic rocks of the non-metamorphic Tuscan Succession are broadly exposed (Fig. 2). They consist of Late Triassic–Cretaceous carbonate-siliceous and Cretaceous–Early Miocene pelagic-turbiditic successions (Losacco, 1952; Losacco and Del Giudice, 1958; Decandia and Lazzarotto, 1972; Lazzarotto, 1973; Bernoulli et al., 1979; Kalin et al., 1979) (Fig. 3).

The Rapolano fault dissected both the Pliocene sediments and the Tuscan Nappe carbonate and pelagic-turbiditic successions. Faulting began during the Zanclean and ended in the Piacenzian. Its maximum vertical displacement is greater than 500 m, based on evidence from geological cross-sections and seismic reflection profiles (Brogi, 2002).

Pleistocene–Holocene travertine masses and active thermal springs are aligned along the Rapolano Fault, where these structures have been dissected by Quaternary normal faults (Brogi, 2004). Hydrothermal fluid circulation began during the Pleistocene and is ongoing, with widespread upwelling of hydrothermal fluids (39 °C) and CO_2 leakage (Baldi et al., 1992; Minissale et al., 2002).

3. Fault zone architecture

The structural architecture of 13 normal faults dissecting the Jurassic radiolarites and affected by widespread hydrothermal alteration have been investigated mainly in two areas (Area 1 and Area 2 in Fig. 4) in the surroundings of the Rapolano area. These faults, Pliocene–Pleistocene in age, are minor structures related to the Rapolano Fault activity (Area 1) and later faults which dissect the Rapolano Fault (Area 2).

Area 1 is characterised by normal faults (pitch ranging from 90° to 65°) with displacements ranging from 1 to 10 m, while Area 2 is typified by a main normal fault with displacement exceeding 10 m (30–40 m as estimated by cartographic data) (Fig. 5), and minor faults with metre displacement.

All the considered fault zones are characterised by three main architectural components: (a) a fault core where most of the slip is accommodated (Chester and Logan, 1986; Chester et al., 1993; Bruhn et al., 1994; Caine et al., 1996; Peacock et al., 2000); (b) a damage zone characterised by complex fracture networks and minor faults (Chester and Logan, 1986; Chester et al., 1993; Bruhn et al., 1994; Caine et al., 1996; Peacock et al., 2000; Peacock, 2002; Jourde et al., 2002); (c) a protolith corresponding to the host rock which records only previous (pre- normal faulting) deformation.

3.1. Protolith: Rock fabric and lithology

The Jurassic siliceous rocks belong to a stratigraphic succession, up to 150 m thick, known as the Diaspri Fm (Kalin et al., 1979) (Fig. 3). This succession shows different lithological characteristics from the top to the bottom. The basal part (about 10 m thick) is mainly characterised by thinly-bedded (average 4–6 cm), highly siliceous, reddish to brownish limestones interbedded with shaly levels about 0.5–1 cm thick. Above, green, reddish and yellow stratified chert beds (average 5–15 cm) occur. The chert beds are rhythmically interbedded with shaly levels up to 2 cm thick. Some chert beds are pure and vitreous, but other beds are characterised by radiolarian chert (radiolarian packstone to grainstone) often laminated at the base of the strata. This succession is overlain by about 10 m of slightly calcareous radiolarian chert beds, about

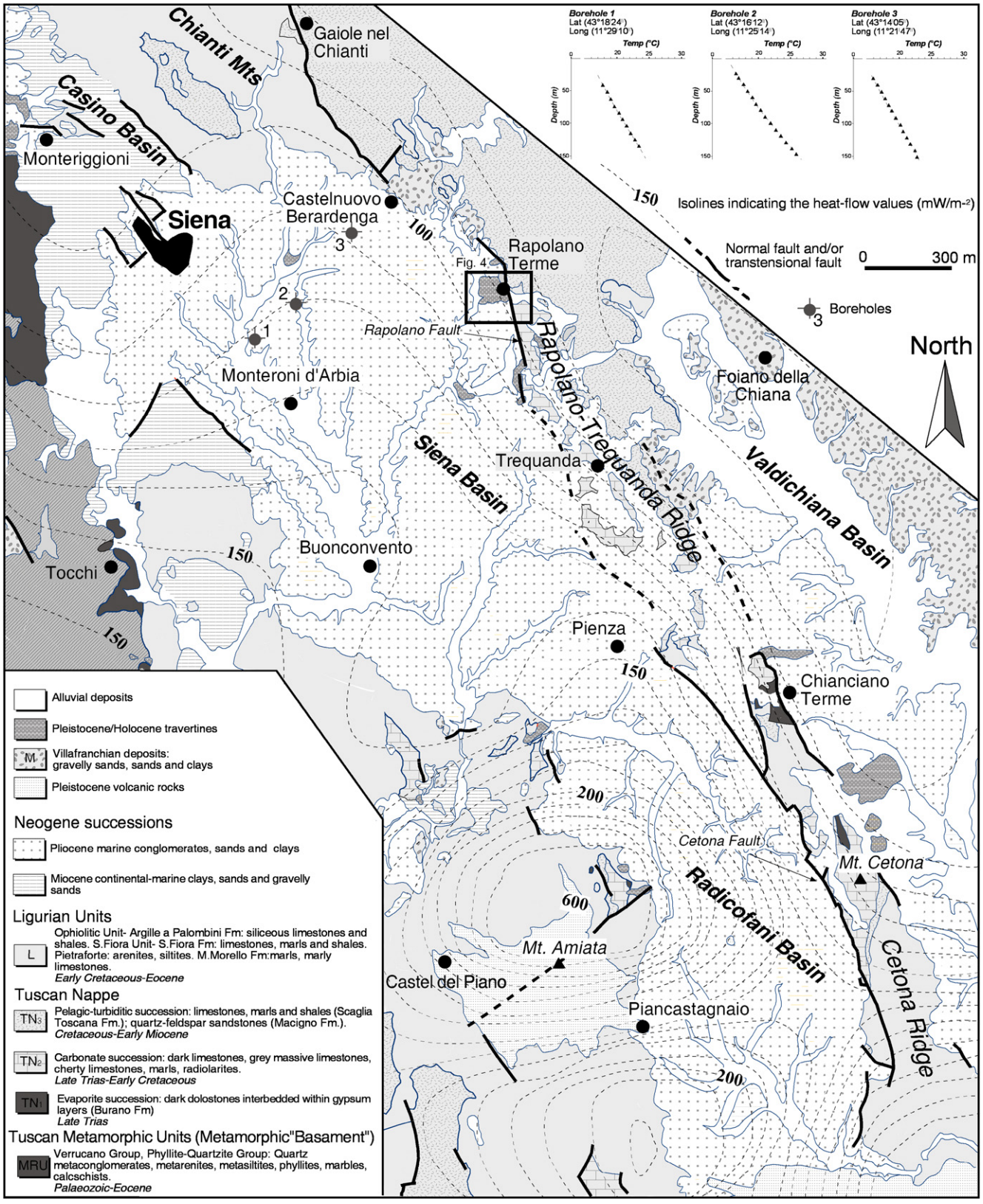

Fig. 2. Geological sketch map of the Siena-Radicofani Basin where the Rapolano Terme area is located. The heat-flow values and contours are modified from Mongelli and Zito (1991). The black rectangle indicates the enlarged area given in Fig. 4. The temperature vs. depth, as recorded in the three boreholes, is also shown (from Mongelli et al., 1982, modified).

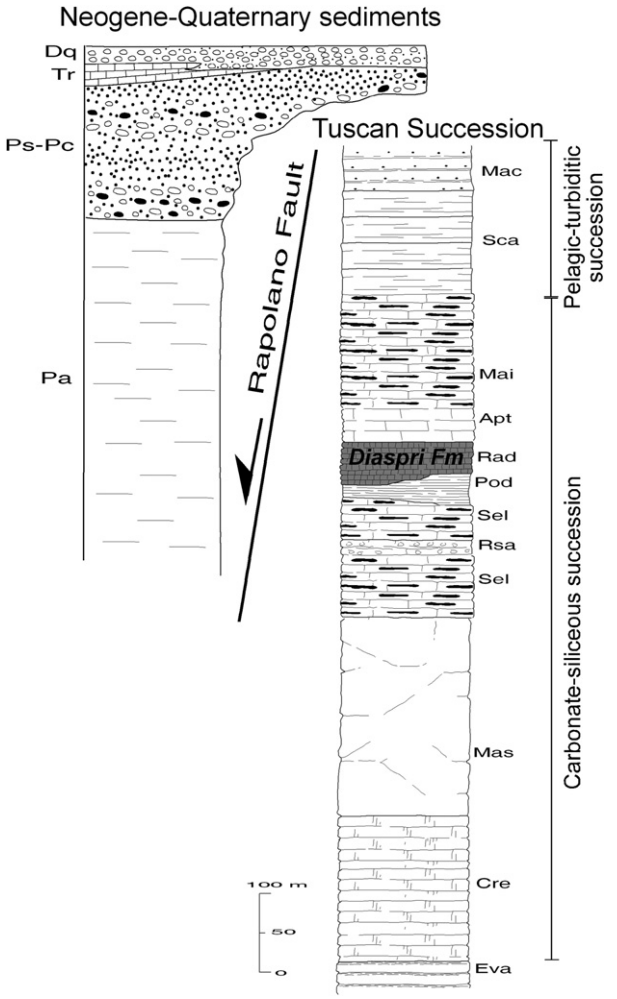

Fig. 3. Tectono-stratigraphic relationships between the Neogene and pre-Neogene successions exposed in the Rapolano Terme area (from Brogi, 2004). Key: Eva, Burano Fm (Late Trias) (only drilled); Cre, Calcari a *Rhaetavicula contorta* Fm (Late Trias); Mas, Calcare Massiccio Fm (Early Lias); Sel, Calcare Selcifero Fm (Middle–Late Lias); Rsa, Calcare Rosso ammonitico Fm (Late Lias); Pod, Marne a *Posidonomya* Fm (Dogger); Rad, Diaspri Fm (Malm); Apt, Calcari ad Aptici Fm (Malm–Early Cretaceous); Mai, Maiolica Fm (Early Cretaceous); Sca, Scaglia Toscana Fm (Early Cretaceous–Oligocene); Mac, Macigno Fm (Late Oligocene–Early Miocene); Pa, marine clays (Early–Middle Pliocene); Ps-Pc, marine sands (Ps) and conglomerates (Pc) (Early–Middle Pliocene); Tr, travertines (Pleistocene–Holocene); Dq, continental gravels, sands and clays (Pleistocene–Holocene).

10–20 thick, with interbedded siliceous grey to yellow shales. Towards the top, this succession grades into the increasingly more calcareous strata belonging to the Calcari ad Aptici Fm (Fig. 3).

This succession suffered strong deformation during the tectonic evolution of the Northern Apennines. Oligocene–Early Miocene compressional tectonics gave rise to fold and thrust systems which deformed the Tuscan Nappe, as well as the tectonic units of the Northern Apennines (Carmignani et al., 1994; Brogi et al., 2005a,b). The siliceous rocks of the Diaspri Fm were strongly fractured. In particular, regularly-spaced joints perpendicular to the bedding are commonly distributed within this succession (Fig. 6). Fractures consist of closely-spaced surfaces crossing only the cherty strata. Within the shaly layers interbedded in the chert, cleavage becomes a pervasive foliation at a very low angle with respect to the bedding.

Damage related to faulting increases the fracture density (see next sections); additional fractures reduce the original size of the rock lithons. In some cases, depending on the stress field orientation, previously developed mechanical surfaces (i.e. tectonic foliations developed during previous deformation: Elter and Sandrelli, 1995; Bonini, 1999; Brogi et al., 2002; Carosi et al., 2004) have been reactivated. In order to define the fracture setting related to the deformations developed before Pleistocene faulting, the fracture density of unfaulted outcrops occurring in the surroundings of the Rapolano area has been considered (Fig. 6) and compared with the data from the study fault zones (see next sections).

3.2. Fault core

The fault core is the zone where the maximum shear deformation is accommodated during faulting, as suggested by the widespread grain size reduction. It divides the footwall and hangingwall damage zones, where fracture networks deform the protolith.

The fault core widths are between 1 and 25 cm, depending on the displacement of the faults. The maximum width has been recorded in the normal fault occurring in Area 2 (Fig. 5).

All fault cores are characterised by cohesive fault rocks with random fabric, characterised by tectonic reduction in grain size and cementation due to mineral precipitation induced by fluid circulation during faulting. Following their textures (classification of Sibson, 1977), the fault rocks can be defined as crush breccia (0–10% matrix, fragments >0.5 cm), fine crush breccia (0–10% matrix, fragments >0.1 cm and <0.5 cm), protocataclasite (10–50% matrix), cataclasite (50–90% matrix) and ultracataclasite (90–100% matrix). Crush breccia and fine crush breccia are the main fault rocks characterising the fault cores where metre displacements occur. A more complex and articulated fault core architecture characterises the fault occurring in Area 2. This fault shows a fault core in which two different domains (SD_1 and SD_2), laterally discontinuous (Fig. 7A,B), can be recognised. The first domain (SD_1) coincides with the slip zone where the main tectonic process was grain reduction. The slip zone has a preserved thickness up to 12 cm. Widespread internal fault rock zonation within the SD_1 has been observed (Fig. 8A). The zoned fault rock is composed of mixtures of quartz and oxides, and ranges from ultracataclasite to protocataclasite at the edges. Protocataclasite and ultracataclasite layers display subangular porphyroclasts of quartz in a brown (iron oxides) matrix (Fig. 9b,c). The ultracataclasite layer is 1–6 cm thick and is distinguished by extremely fine grain size, absence or scarce presence of porphyroclasts, and locally developed, irregularly spaced, parallel shear planes (from 1 to 10 mm) which produced a widespread crenulation fabric (Fig. 9d).

The second domain (SD_2), about 10–15 cm in width, consists of well-defined C_1-type shear planes (Riedel shear meshes in Tchalenko, 1970 and Sibson, 1996) defining

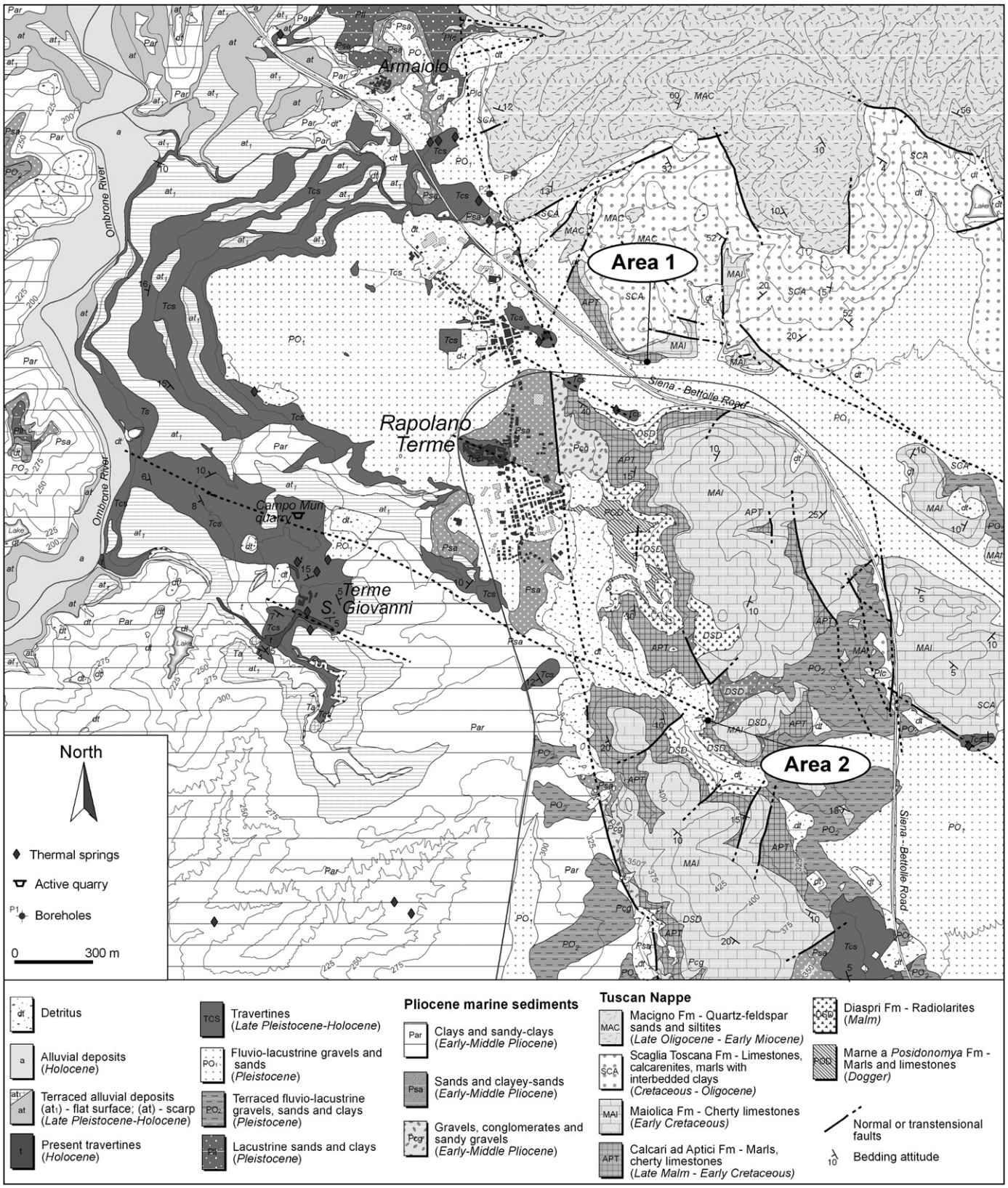

Fig. 4. Detailed geological map of the study area. Area 1 and Area 2 indicate the areas where the structural analyses of the fault zones have been carried out.

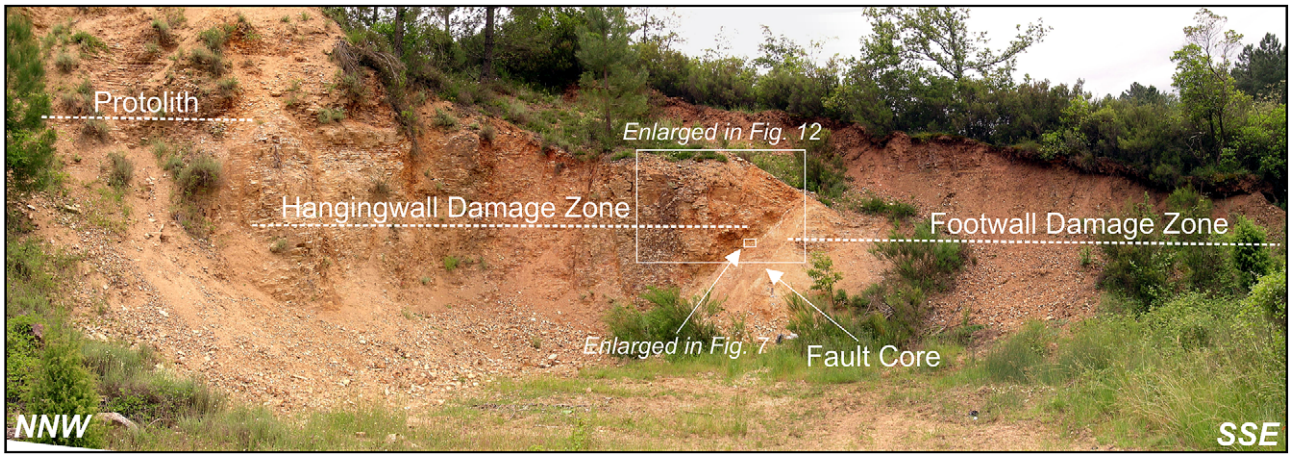

Fig. 5. The fault zone within the Jurassic siliceous succession (Diaspri Fm) exposed in Area 2. See Fig. 4 for location. Details from the damage zone and fault core are given in Figs. 7 and 12.

centimetre lithons preserving relict fractures probably reactivated during shearing (Fig. 7). Cataclasites and protocataclasites are the main fault rocks typifying this domain, where rocks profoundly altered by hydrothermal fluids occur (see the next section). Shear plane spacing ranges from several centimetres to some decimetres. The orientation of these shear planes is consistent with fault plane striking and down-dip movements (Fig. 9a,b). The transition zone from SD_1 and SD_2 domains is gradational at the microscopic scale, characterised by discontinuous lenses of cataclasite that is highly altered by fluid circulation.

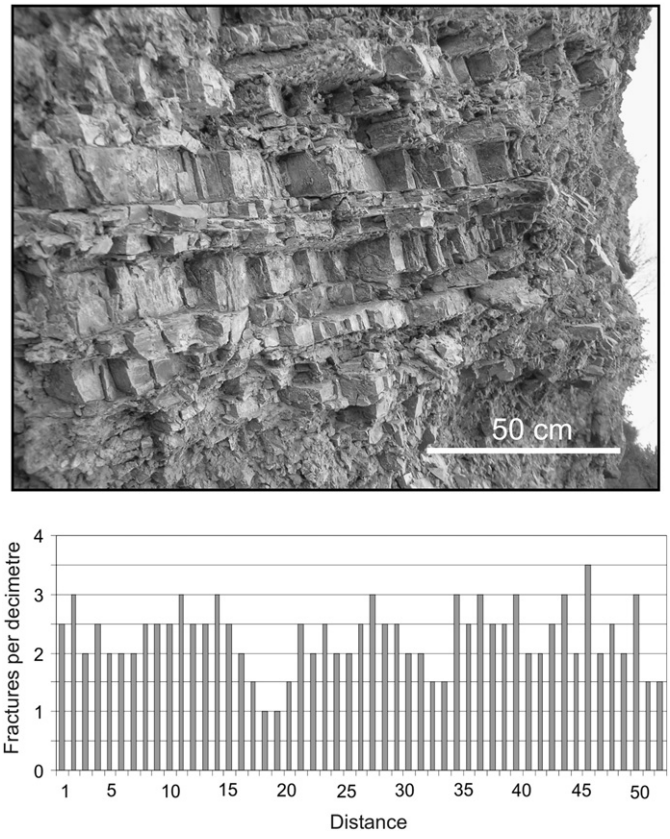

Fig. 6. Fracture distribution within the Jurassic siliceous succession (Diaspri Fm) characterising the protolith far from the fault zones. These fractures have a homogeneous distribution because they are related to deformational events which took place during the tectonic evolution of the Northern Apennines.

3.3. Damage zone

The damage zone is the deformed rock volume surrounding the fault core. The damage zone consists of a well-developed fracture set and minor normal faults, which affected the protolith during faulting. The fracture density reaches the maximum value close to the fault core and decreases with the distance from the slip zone. The intensity of deformation within the damage zone has been quantified by scan line measurements of the fractures and minor faults (Figs. 9 and 10). These measurements include orientation parameters and the qualification of fault-related features, as well as information on the spatial distribution of the different discontinuity sets recognised in outcrop. Scan-line measurements have been performed across the fault zones, on the plane defined by the σ_1 and σ_3 stress tensors of the normal faults, and orthogonal to the σ_2.

Fracture analyses were realised in continuous outcrop exposures in the two representative areas located along the Rapolano Fault, where these structures have been dissected by Pleistocene normal faults. Fig. 9 shows the scan line of the most representative measured fault, exposed in Area 2 (Figs. 4 and 7). Fracture data recorded from areas 1 and 2 were plotted on rose diagrams and frequency distribution histograms (Fig. 10) to compare orientations, changes in fracture density and permeability structures (Fig 11). Permeability structure is defined following the Caine et al. (1996) concept, as illustrated in the next paragraph. Hydrothermal alteration of the host rock widely characterises the fractures. Frequently the fractures are infilled by minerals (carbonates, oxides and sulphides) deposited during hydrothermal fluid circulation (see below), attesting to a significant volume of fluids circulating through the fault zones.

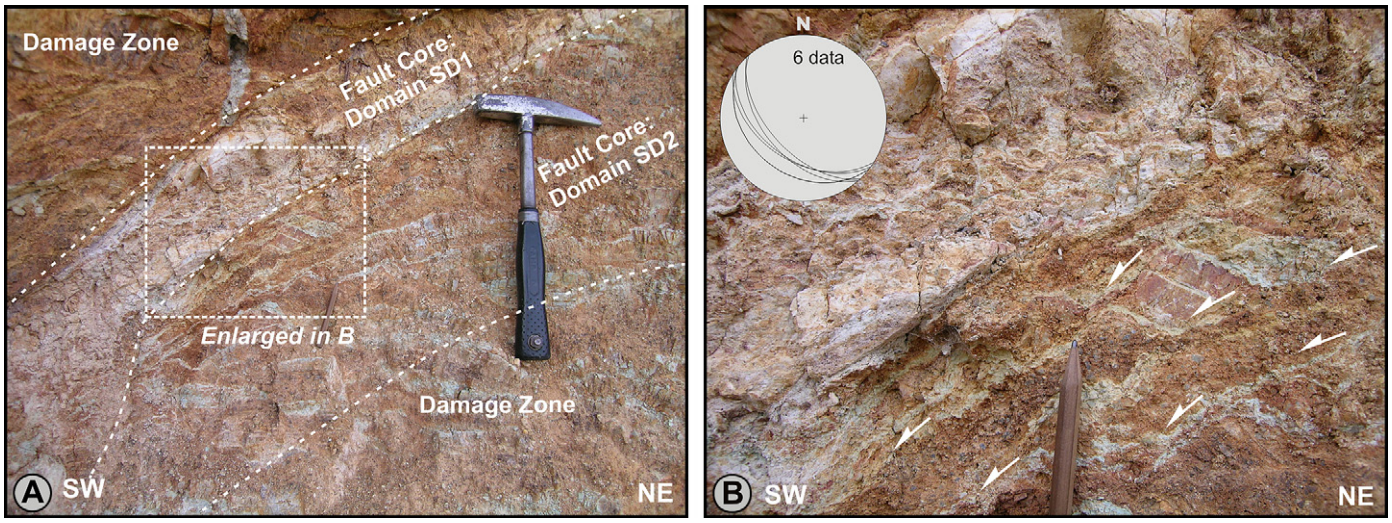

Fig. 7. Detail of the fault core belonging to the fault illustrated in Fig. 5. The fault core consists of two domains as discussed in the text. The stereographic diagram (Schmidt diagram, lower hemisphere) indicates the shear planes illustrated in B. The sense of shear is indicated by the white arrows.

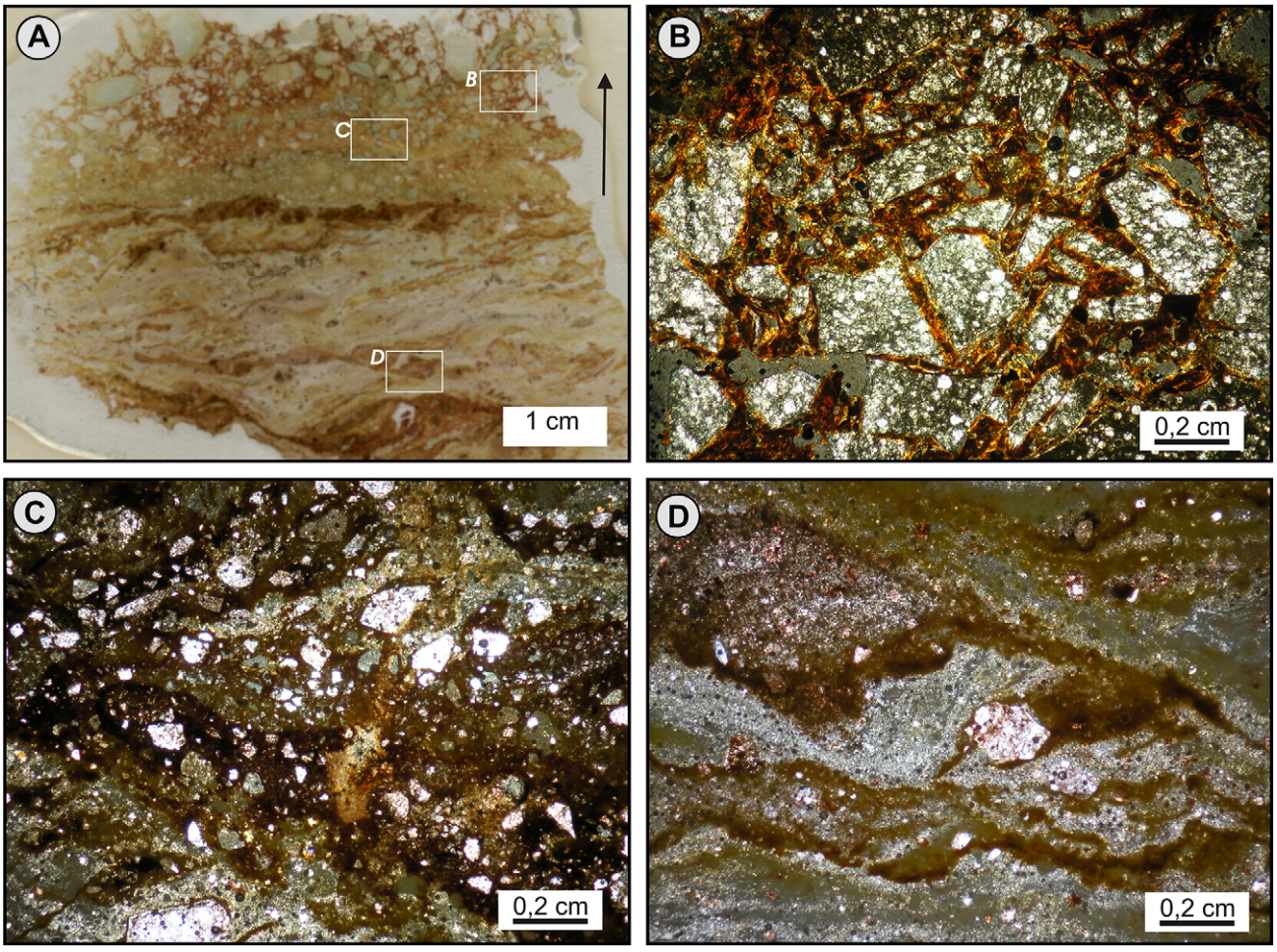

Fig. 8. Photomicrographs (plane-polarised light) of thin-sections from fault rock samples collected in the fault core, domain D_1, of the fault exposed in Area 2. (A) Graded fault rock of domain D_1 shown in Fig. 7; the arrow indicates the passage from ultracataclasite to cataclasite. (B) Detail of the cataclasite, formed by fragments of radiolarites. (C) Grain reduction progressively occurs towards the ultracaclasite. (D) The ultracataclasite is typified by shear planes coherent with the fault kinematics; pseudo-hexagonal radiolarite fragments can be locally recognised.

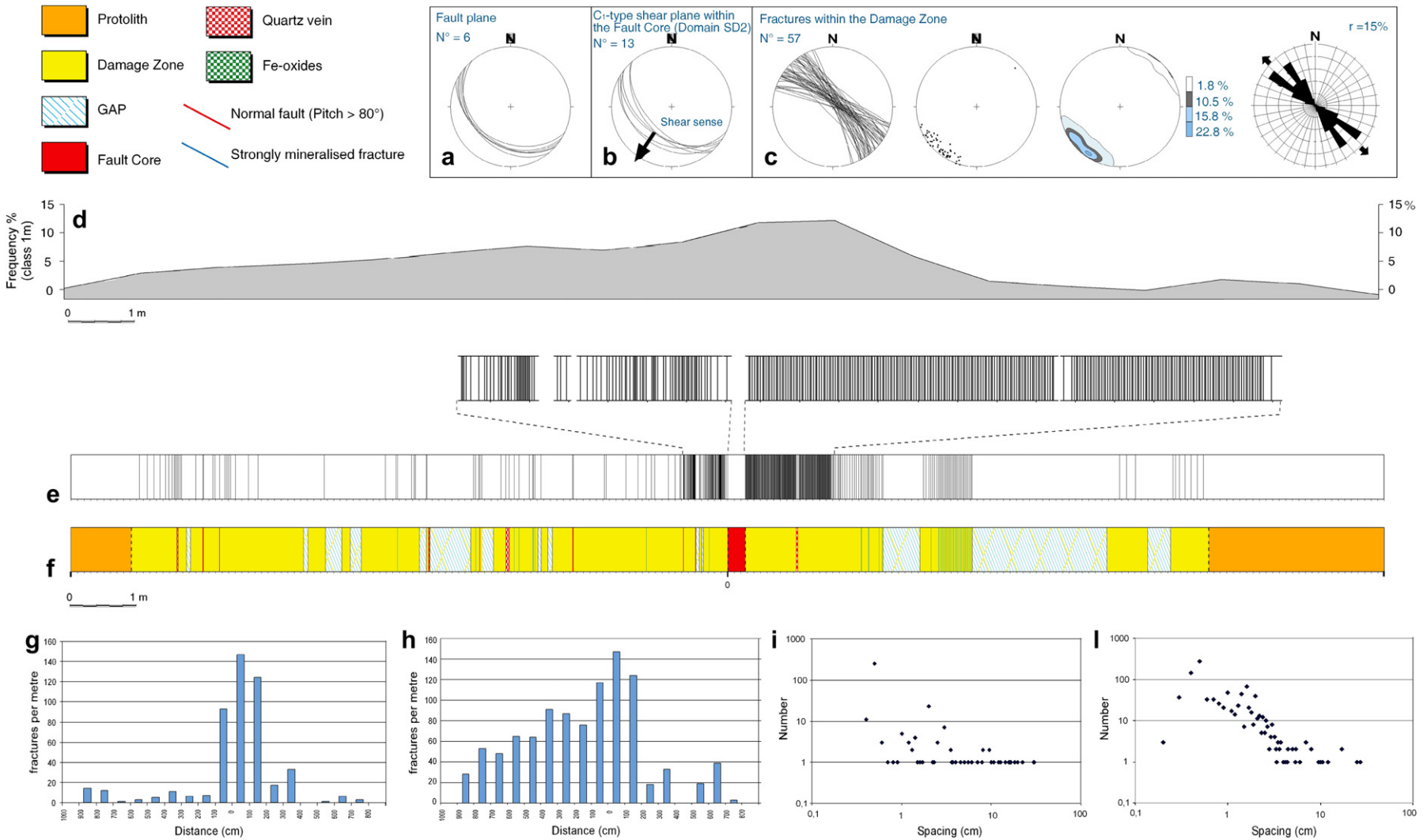

Fig. 9. Scan line across the fault zone exposed in Area 2 shown in Fig. 5. Structural information concerning kinematics, geometry and density of fractures are illustrated in the diagrams a–l: the equal-area plots (Schmidt diagram, lower hemisphere) indicate: (a) the great circles of the fault plane; (b) the cyclographic traces of the C_1-type shear planes occurring within the domain SD_2 of the fault core (see Figs. 7 and 15); (c) the cyclographic traces, poles, contouring of poles and rose diagram of the fractures occurring in the damage zone. (d) Diagram showing the frequency distribution of the fractures (spacing 1 m) in the damage zone; (e) position of the fractures and minor faults within the fault zone; (f) lithological information of the fault zone; (g) histograms indicating fractures (spacing 1m) vs. distance; (h) histograms indicating fractures, minor faults and relict fractures (spacing 1 m) vs. distance; (i) fractures (spacing 1 m) vs. spacing; (l) fractures, minor fault and relict fractures vs. spacing.

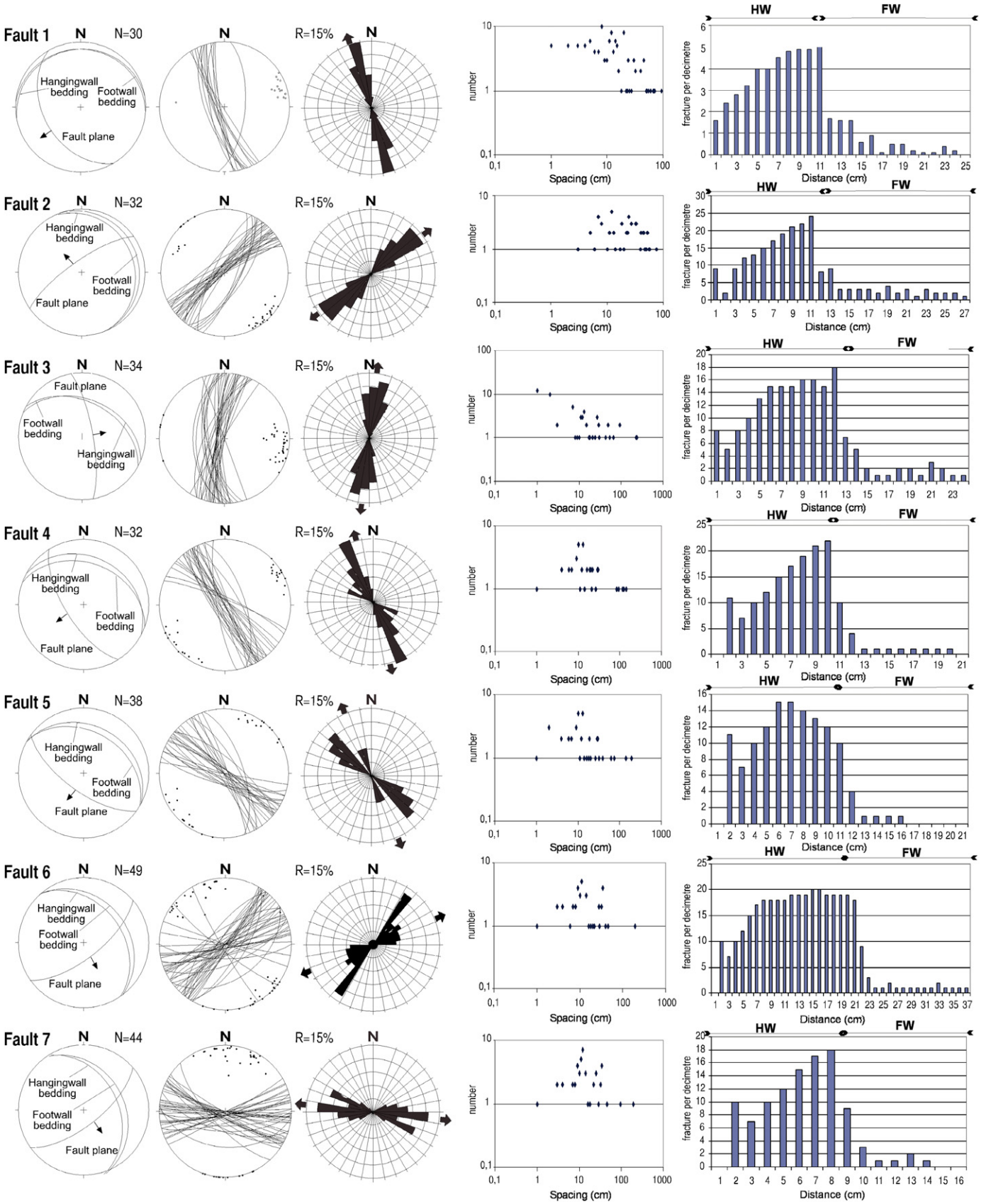

Fig. 10. Structural information (stereographic diagrams, Schmidt diagram (lower hemisphere) and statistical diagrams) of the analysed fault zones from Area 1 (see Fig. 4 for location). For each numbered fault, it is shown, from the left: cyclographs of the fault plane with related pitch (arrow) and bedding in the hangingwall and footwall; cyclographs and poles of the fracture planes; rose diagram of the fractures; diagram showing the number of the fractures vs. spacing; diagram showing the number of fractures (per decimetre) vs. distance (FC: fault core; FW: footwall; HW: hangingwall).

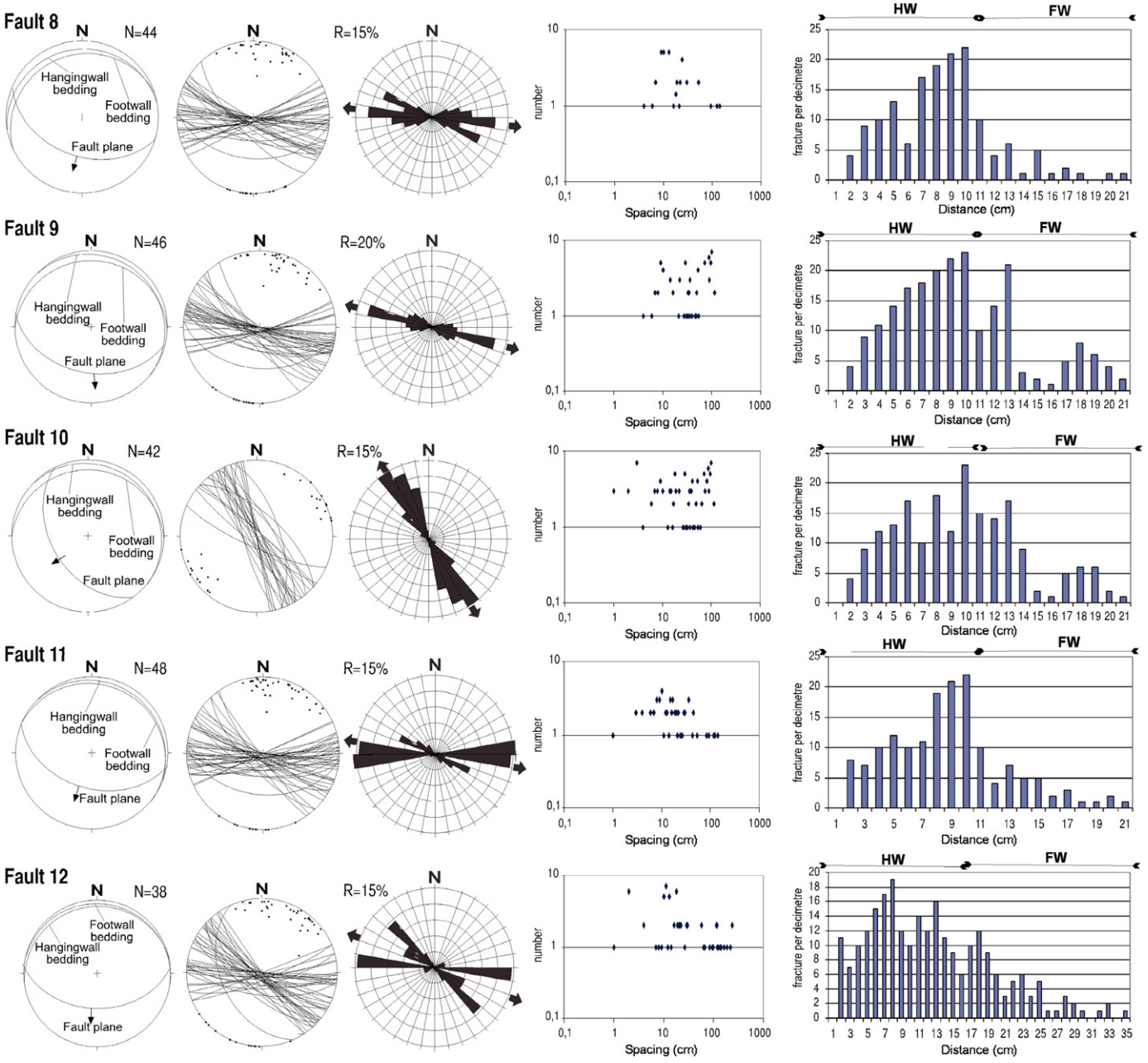

Fig. 10 (*continued*).

All the considered damage zones are characterised by similar geometric settings of the fracture network, which show a dominant fracture set forming an angle of about 40–45° with respect to the slip surface (Fig. 12). Close to the fault core, minor fractures parallel to the fault plane are locally developed. Pre-existing fractures were often overprinted by the later fault-associated fractures.

All the damage zones are characteristically asymmetric. Fractures are better developed in the hangingwall blocks, especially for faults with displacements exceeding 10 m (Figs. 9 and 10). In addition, the damage zone occurring in the hangingwall is wider then in the footwall. Also, fractures are regularly spaced in the hangingwall, and their density increases rapidly toward the fault core. In contrast, fracture density in the footwall is more complicated, with no discernible density decrease away from the slip zone (Figs. 9 and 10). The fracture spacing is of the order of a few centimetres (1–5 cm) to some decimetres (Fig. 12). The resulting fracture network in the damage zone generates a rock fabric consisting of lithons a few centimetres in size (1–20 cm) showing relict fractures, probably reactivated.

Good exposure in fresh-cuts occurring in Area 2 allow us to analyse the 3D fracture network and related permeability for a normal fault (fault no. 14 in Fig. 11), showing widespread mineralisation and hydrothermal alteration mainly consisting of iron oxide reduction. Two natural sections across the fault zone, perpendicular and parallel to the strike of the fault plane, have been observed. The section parallel to the strike of the

Fault Number	Fault Zone width	Damage Zone width	Fault Core width	*Fa* parameter	Location
1	250	245	5	0,98	Area 1
2	253	250	3	0,988142292	Area 1
3	210	205	5	0,976190476	Area 1
4	161	160	1	0,99378882	Area 1
5	84	80	4	0,952380952	Area 1
6	357	350	7	0,980392157	Area 1
7	68,2	68	0,2	0,997067449	Area 1
8	75	73	2	0,973333333	Area 1
9	119	118	1	0,991596639	Area 1
10	125,5	124	1,5	0,988047809	Area 1
11	214	210	4	0,981308411	Area 1
12	329	323	6	0,981762918	Area 1
13	1634	1607	27	0,983476132	Area 2

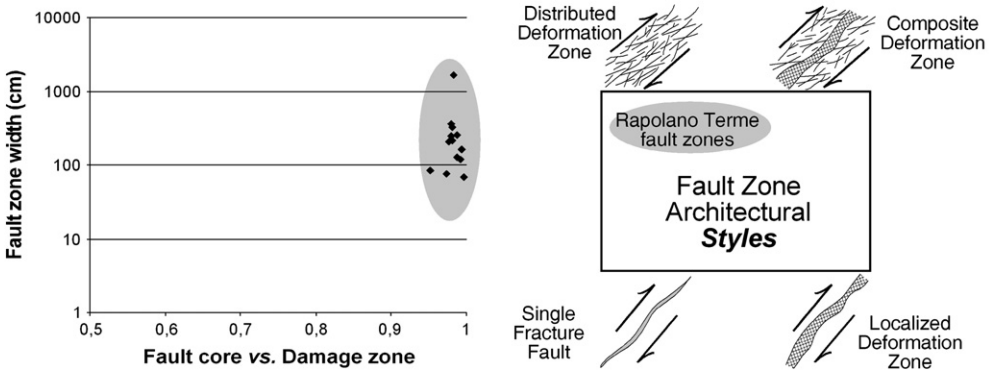

Fig. 11. Permeability diagram from Caine et al. (1996) and geometric parameters of the indicated fault zones.

fault plane is only characterised by fractures which correspond to relict cleavage. The fractures developed during faulting are about parallel to the section plane, and thus they are not observed from this point of view. By contrast, the intensity of deformation related to faulting has been measured along the section perpendicular to the strike of the fault plane, shown in Fig. 5.

According to the trend of the Pleistocene normal faults affecting the Rapolano area, the measured faults range from NW–SE to SW–NE striking (Figs. 9 and 10). Fracture

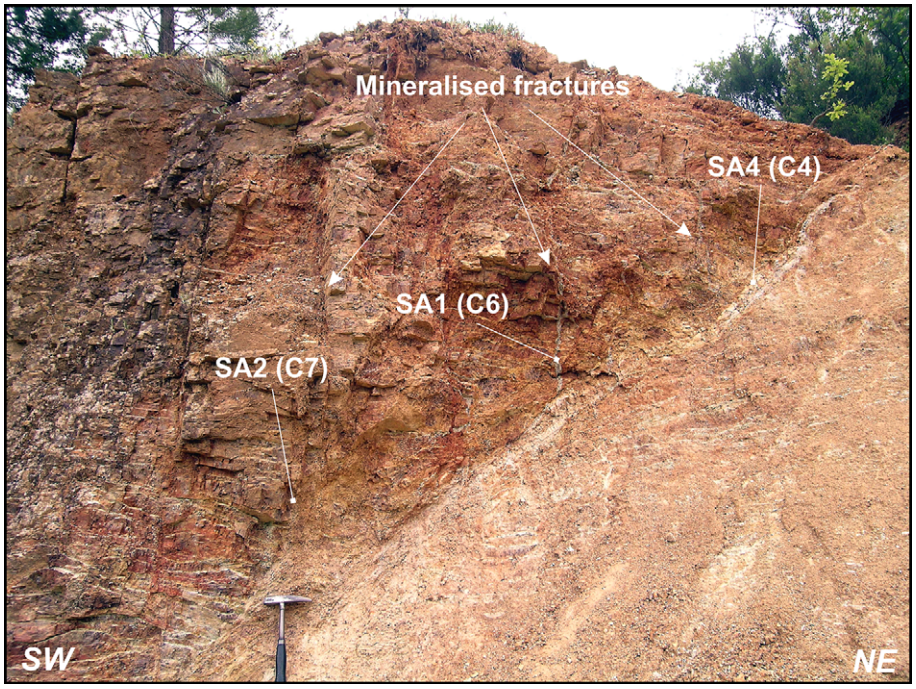

Fig. 12. Detail of the fracture set occurring in the hangingwall damage zone. The fractures have been deeply altered by fluid circulation; the locations of the analysed samples given in Fig. 16 are also shown. More information is given in the text.

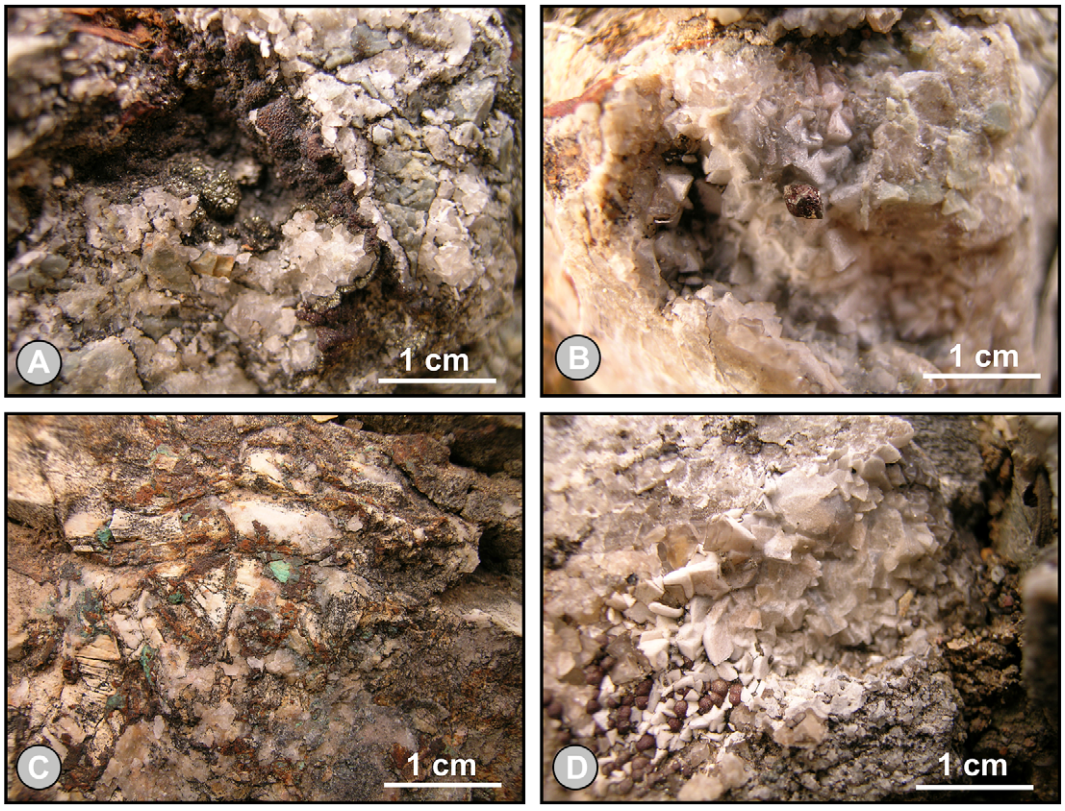

Fig. 13. Mineralogical associations related to extraformational fluid circulation along the fault zones. (A) Globular marcasite and calcite; (B) dolomite and marcasite crystals; (C) malachite, calcite and iron oxides; (D) dolomite, calcite and globular marcasite.

orientation in their damage zones is roughly parallel to the strike of the fault planes, according to the normal fault kinematics.

Minor normal faults with centimetre to decimetre displacements mainly occur in the hangingwall damage zones. These faults have striated and clean surfaces showing a parallel strike with respect to the main fracture set and fault core.

4. Permeability structure and hydrothermal alteration

All recorded fault zones are characterised by intense fracturing and hydrothermal alteration, suggesting good permeability related to faulting. Hydrothermal circulation is a consequence of fluids deriving from meteoric waters and circulating in carbonate and sulphate rocks (Minissale et al., 2002). Their thermal condition is due to the anomalous geothermal gradient (Mongelli et al., 1982; Mongelli and Zito, 1991).

The damage zones are characterised by fractures infilled by minerals such as carbonates (calcite, dolomite, malachite, azurite), quartz, iron sulphide (marcasite) and oxides (goethite, limonite) (Fig. 13). Centimetre haloes typify the fracture edges, indicating iron oxide reduction of the host rocks (Fig. 14). Alteration is concentrated along mesoscopic fractures, but locally also occurs along smaller cracks, isolating centimetre lithons. These fractures are locally infilled by quartz and oxides

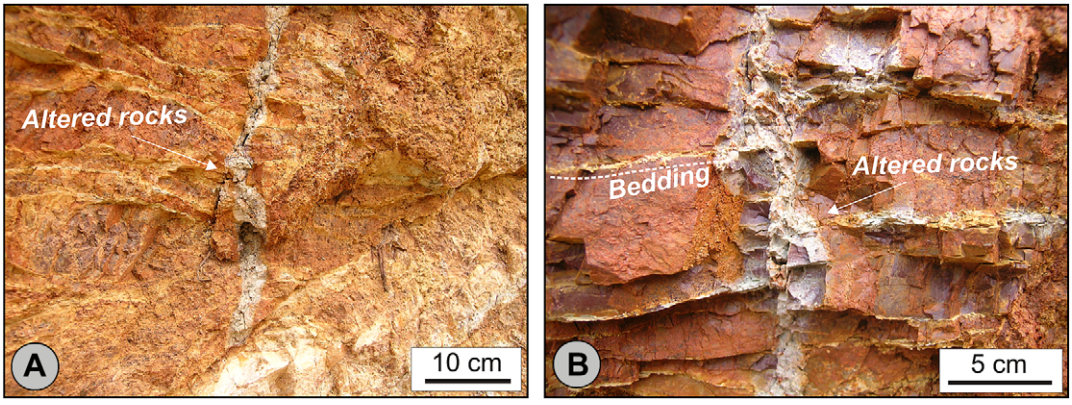

Fig. 14. (A) Fluid circulation along the fractures occurring within the damage zone gave rise to haloes indicating iron oxide reduction of the horst rocks (see text for more details). (B) Fluid circulating along the fractures penetrated between the strata, producing widespread alteration of the shaly layers.

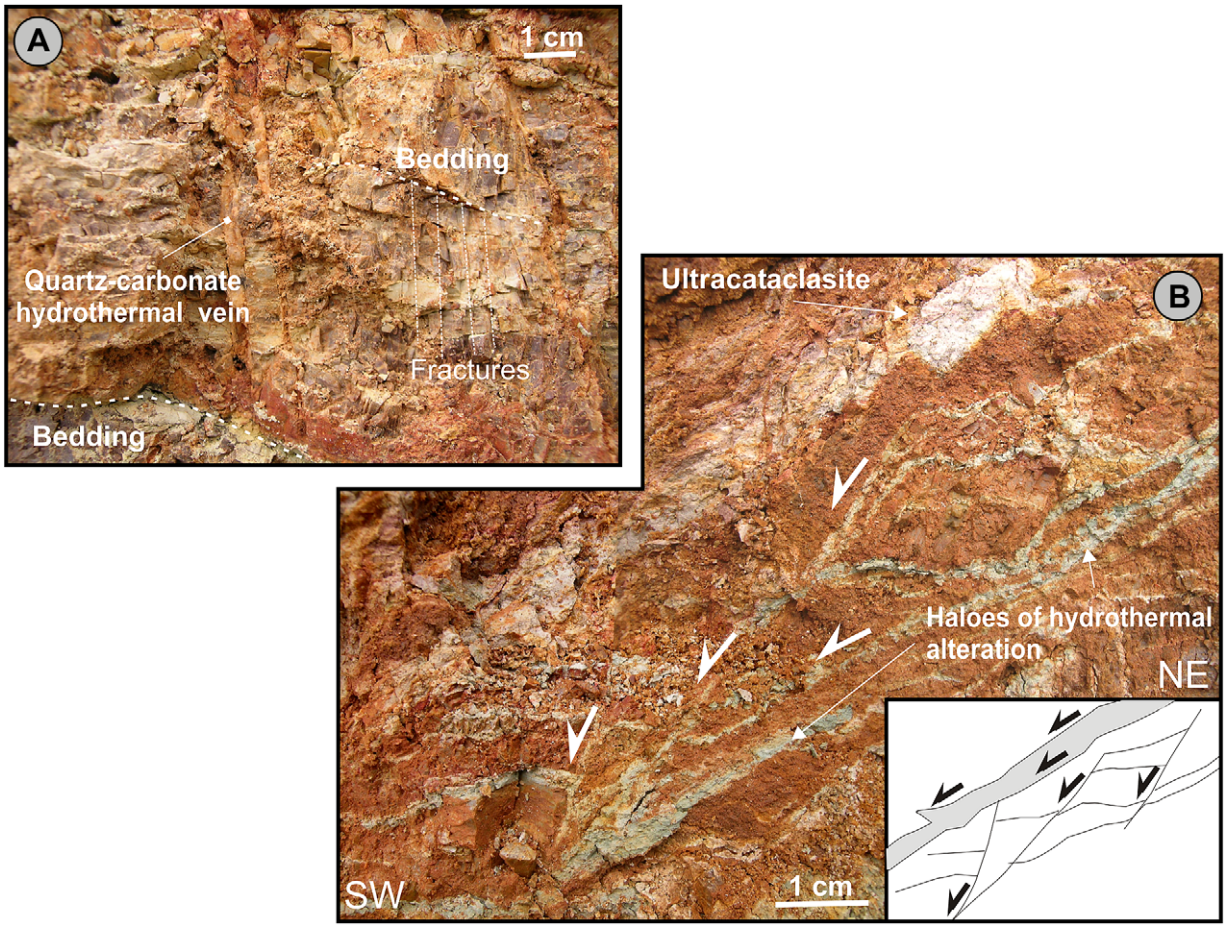

Fig. 15. Hydrothermal alteration and minerals characterising both the damage zone and fault core. (A) Hydrothermal quartz veins fill fractures within the damage zone. (B) Hydrothermal alteration characterises the C_1-type shear planes occurring within domain SD_2 of the fault core.

(Fig. 15A). The numerical measures of the fault zones using the parameters introduced by Caine et al. (1996) allow us to evaluate the permeability structure for the analysed faults (Fig. 11). Combined conduit–barrier and distributed conduit are the main conceptual mechanisms driving the fault-related fluid flow in the study area.

The fault cores are characterised by cemented rocks. Cementation is due to quartz and iron oxide precipitation during the latest stage of faulting. At Area 1 the mineralogical alteration of the fault cores is extensive, mainly caused by the precipitation of quartz, marcasite and iron oxides. The permeability of the fault core was at a maximum during the initial stage of faulting: progressive fracturing concentrated within the shear zone, favouring fluid circulation. Nevertheless, the subsequent grain-size reduction produced by progressive deformation within the slip zone of the fault reduced the permeability. By contrast, the permeability of the damage zone is strictly related to the hydraulic proprieties of the fractures (i.e. width, interconnectivity, frequency, etc.) mainly developed in the latest stage of faulting. This produced high permeability within the damage zone for extra-formational fluid circulation.

The core and damage zone components of the fault zones are surrounded by the protolith, where fault-related permeability structures are absent.

X-ray powder diffraction (XRD) analyses of selected samples aided in the identification of the mineralogy of the altered rocks, both in the core faults and in the damage zones. Hydrothermal alteration has been investigated in the fault zone exposed in Area 2 (Fig. 11). As shown by the diffraction analyses, the haloes of iron oxide reduction along the fractures in the damage zone show a similar mineralogy to the host rocks (Fig. 16a,b). This can be explained by the circulation of extra-formational fluid through the fractures. In fact, it is known that iron oxide reduction in the host rocks implies the mobilisation of Fe^{3+} within the haematite by an iron-reducing fluid. Extra-formational fluids capable of reducing iron oxides have been identified as containing hydrocarbons, organic acids, methane and/or hydrogen sulphide (Chan et al., 2000; Parry et al., 2004; Dockrill, 2005). On the basis of the geochemical characteristics of the hydrothermal fluid circulating in the Rapolano thermal area (Minissale et al., 2002), neither hydrocarbons nor organic acids or methane could be considered responsible for the iron oxide reduction. Only hydrogen sulphide is abundantly contained in the fluids, which presently are characterised by temperatures reaching a maximum of 40 °C. Fluids with high hydrogen sulphide contents, circulating along the fault zone, interacted with the calcareous beds which are rarely interbedded within the siliceous

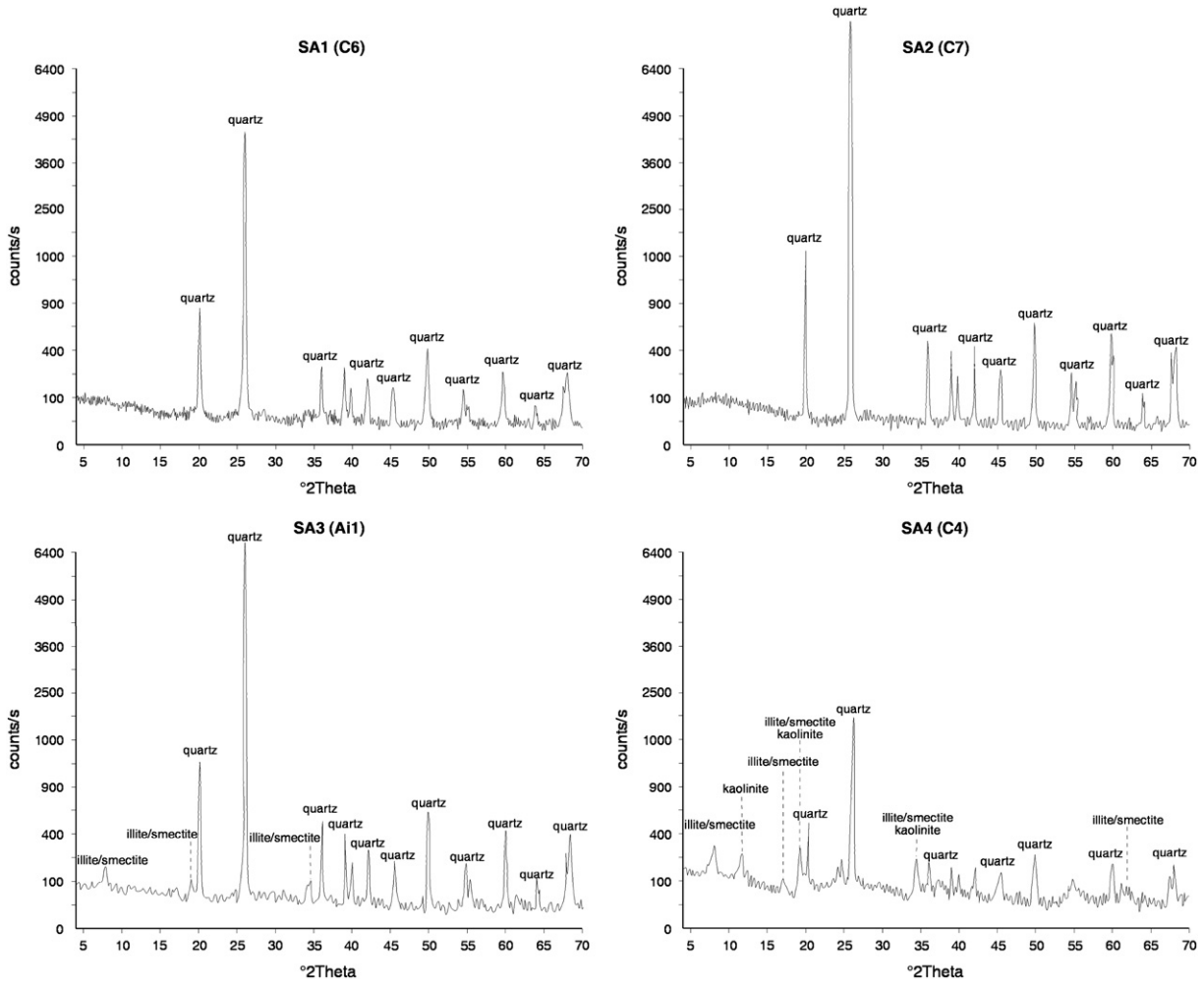

Fig. 16. X-ray diagrams of collected mineralised samples. Locations of SA1, SA2 and SA4 are given in Fig. 11. See the text for more details.

strata. As a consequence, the calcareous rocks were decarbonated and their hydrothermal alteration product is yellowish or white siliceous clay, industrially exploited for ceramic production (Fig. 17). The siliceous strata become whiter close to the fractures. XRD analyses of these hydrothermally altered rocks reveal a composition characterised by quartz and illite/smectite (Fig. 16c). Illite/smectite, quartz and kaolinite minerals with sporadic amounts of calcite, dolomite and haematite are also found in the fault cores. In particular, a mineralogical assemblage consisting of quartz, illite-smectite and kaolinite has been recognised within domain SD_2 of the fault core, sampled in Area 2 (Fig. 16d). The increase in illite/smectite and kaolinite minerals commonly occurs where the fault rocks are more altered, principally along the minor shear planes occurring within domain SD_2 of the fault core (Fig. 15B), indicating a strong interaction between hydrothermal fluids and host rocks.

5. Discussion and conclusion

5.1. Fault zone architecture

Spatial distribution of the fractures and minor faults can be considered in the conceptual fault zone model given in Fig. 18A. At the Rapolano Terme the considered faults developed at shallow depths in the crust, and their architecture agrees with the conceptual model given in Fig. 19A and B. Nevertheless, some differences with respect to the geometric setting of the damage zones described for crystalline and calcareous rocks have been observed. Differences are mainly observed for the damage zones, which play the most important role for the permeability of the fault zone. These differences consist of: (a) exclusive occurrence of a pervasive fracture set at about 45° with respect to the main slip zone (fault core); (b) asymmetrical distribution of the damage zone in the hangingwall and footwall blocks, resulting in the hangingwall damage zone being thicker than in the footwall block. Concerning the fracture network, the faults developed in the Rapolano Terme area agree with the fault architecture described for normal faults occurring in the Brushy Canyon (West Texas), described by Nelson et al. (1999), which affected mainly sandstones. Regarding the asymmetrical development of the damage zone, similarities occur with the Moab normal fault (Utah) described by Berg and Skar (2005), and with some faults occurring in the Valley of Fire State Park (southern Nevada) described by Flodin and Aydin (2004), even if in this latter case they are strike-slip faults.

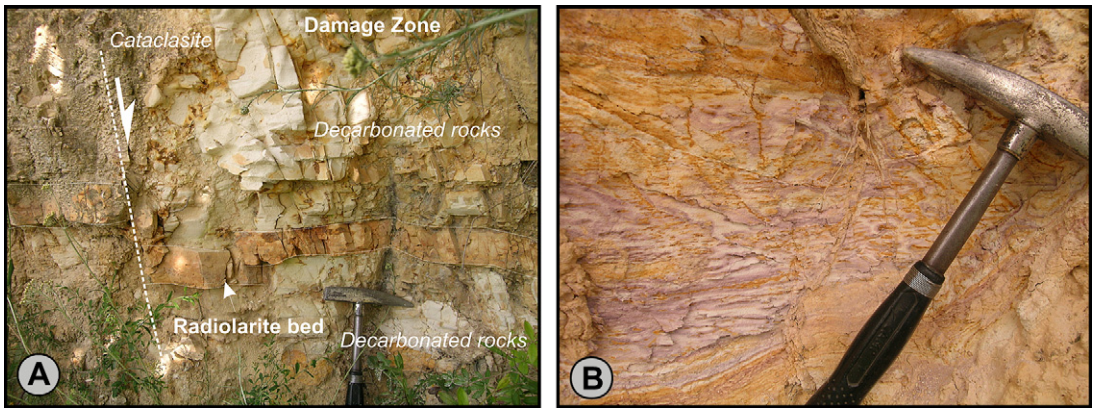

Fig. 17. (A) Detail of the hydrothermally altered carbonate rocks sporadically interbedded within the siliceous strata in the damage zone of normal faults. Alteration produced decarbonation of the calcareous strata; quartz and clayey minerals were concentrated. The X-ray diagram of sample SA3 given in Fig. 16 indicates that clayey minerals consist of illite/smectite. (B) Detail of the altered carbonate rocks.

In both cases, sandstones are the main lithotypes dissected by faulting. Similar features have been observed through numerical experiments carried out for extensional faults (Zhang and Sanderson, 1996). The numerical modelling of the effects of fault slip on fluid flow around extensional faults highlighted that normal faulting at shallow depths can produce dilation and fluid flow mainly in the fault zone and in the hangingwall (Zhang and Sanderson, 1996), showing a reasonable correspondence with observed natural examples from the Rapolano Terme area.

Fault cores in the study areas were produced by brittle deformation. Additionally, minor brittle shear structures occurring within the domain SD_2 show similar characteristics to those given in the conceptual model proposed by Tchalenko (1970) (Fig. 19B).

5.2. Hydrothermal alteration and fluid flow circulation

Mineralisation and hydrothermal alteration within the fault zones indicate high permeability for the studied faults. The conceptual scheme proposed by Caine et al. (1996) has been largely been adopted for quantitative and qualitative characterisation of the permeability structure of fault zones (Cello et al., 2000, 2001a,b). Four end-member fault zone typologies have been recognised in the upper crust. Two end-members represent barriers to fluid flow, whereas other ones correspond to

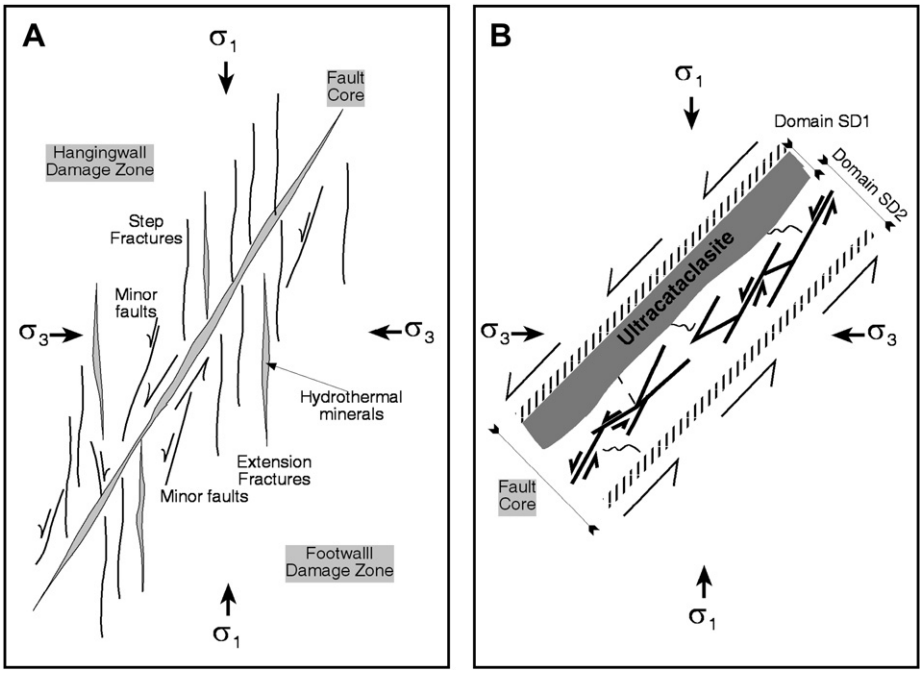

Fig. 18. (A) Cartoon illustrating the fracture network and minor faults associated with normal fault zones as recognised in the study area. (B) Cartoon showing the structure of the fault core as recognised in the normal fault of the study area. The fault core can be divided into two domains: domain SD_1 characterised by ultracataclasite rocks, and domain SD_2 characterised by cataclasite, where minor C_1-type shear planes occur.

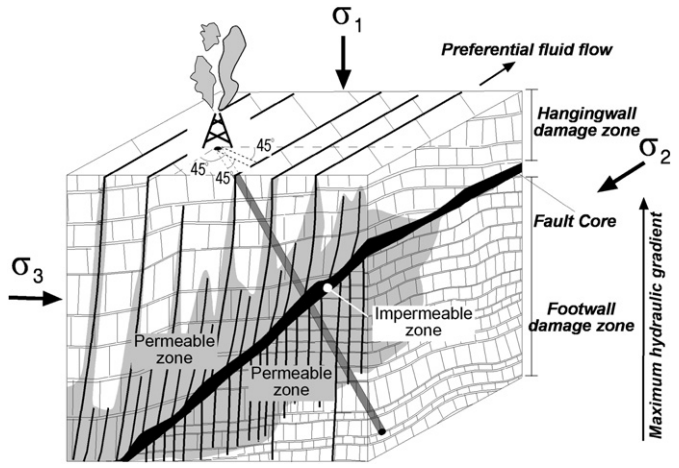

Fig. 19. Idealised block diagram showing the fault zones as documented in the Rapolano area. The grey area indicates hydrothermal alteration due to extra-formational fluid circulation. For geothermal exploitation, the boreholes should be drilled at 45° with respect to the fracture traces, and with respect to the horizontal topographic surface.

conduits for fluid circulation. Following the Caine et al. (1996) scheme, the faults occurring in the Rapolano area are characterised by permeability related to distributed conduits and combined conduit–barrier systems (Fig. 11). This implies that circulation could be mainly concentrated along fractures in the damage zones, because fault cores, especially if cemented (as is the case for the studied faults), represent barriers for fluid circulation particularly in the latest stages of fault activity (Antonellini and Aydin, 1994; Caine et al., 1996; Evans et al., 1997). The fault growth and evolution, due to the shear concentration within the fault core, give rise to progressive grain-size reduction within the slip zone. In this scenario, the damage zones increase in width, involving new protolith in the deformation, while progressive grain-size reduction, dissolution, and mineral precipitation within the fault cores cause reduction of permeability. This implies that fault cores became barriers for fluid circulation.

Hydrothermal alteration and mineral deposition occurred within the fault cores of the analysed faults, suggesting that hydrothermal fluid circulation took place within the fault rocks. Additionally, different fluid compositions characterised the fault cores and the damage zones, as indicated by the different chemical compositions of the mineral deposits. The fluids circulating within the fault cores deposited carbonates (calcite, malachite and dolomite) and produced alteration of the host rocks, giving rise to illite/smectite and kaolinite. In contrast, the fluids circulating within the damage zones were enriched in hydrogen sulphides and became under-saturated solutions in bicarbonates, as suggested by the alteration haloes along the fractures. The fluid enrichment of hydrogen sulphide implies a fluid pathway within the Triassic evaporites (Burano Fm in Fig. 4), mainly composed of sulphate and carbonate lithotypes.

Several fractures show evidence of episodic dilation with precipitation of quartz (Fig. 15A), probably attesting to periods of high fluid pressure.

The different fluid compositions can be explained assuming that extra-formational bicarbonate-rich, supersaturated solutions circulated during the initial stages of faulting. At that time, localised open fractures enhanced the permeability within a restricted fault zone. Successively, fault growth involved new protolith in the deformation; the damage zones increased in width and permeability, while the fault cores become impermeable. As a result, the fluids circulated along the fractures developed both in the footwall and hangingwall damage zones during the latest stages of faulting. Additionally, at that time the fluids changed their composition.

The fracture network of the damage zones is characterised by parallel fractures containing similar alteration products, implying that all fractures developed under the same range of pressure, temperature and fluid composition. Fractures within the damage zones are sub-parallel with respect to the relict fractures affecting the host rocks. This geometric condition caused a pronounced asymmetric permeability within the fault zones, resulting in a maximum along the fracture planes which intersect the fault planes at about 45°. This geometric setting reveals much on the fault zone permeability, which is maximum along-strike of the fault. According to the literature data, the fault-normal permeability is minimal. In fact, hydrothermal alteration mainly occurs within fractures in the footwall damage zones, indicating that the fault core represented a barrier for fluids circulating in the direction perpendicular to the fault plane. Therefore, diffuse hydrothermal alteration took place in the footwall damage zones located close to the fault cores, which stopped the fluids from upwelling. The barrier for fluid flow was probably laterally discontinuous, as attested to by hydrothermal alteration occurring within a vertical fracture set in the hangingwall damage zone (Fig. 12).

5.3. Prediction for low-enthalpy geothermal exploitation

The geometric setting of the fracture networks occurring in the damage zones of the study faults is fundamental for prediction of fluid circulation in this geothermal area, as well as in all other areas where hydrothermal circulation takes place within siliceous sedimentary rocks. The three-dimensional conceptual model of the fault zone fracture network (Fig. 19), coupled with the effects of hydrothermal alteration, confirm that fluid flow within the fault zone agrees with data obtained by reservoir flow simulators and numerical computation (Sibson, 1996; Evans et al., 1997; Caine and Forster, 1999; Jourde et al., 2002) which attest that high-permeability components are represented by fractures and slip surfaces within the damage zones (Caine et al., 1996). By contrast, a much reduced permeability characterises the fault cores. In the study area the permeable elements are subvertical and concentrated close to the fault core. Fluid migration through the fault zone is influenced by 3-D interconnections between existing discontinuities such as bedding, fractures and faults. Considering the fracture orientation with respect to the bedding surfaces, we can suppose that fluid flow is maximum along the intersection of these planar elements, giving rise to conduits about parallel to the fault planes (Fig. 19). In this condition the fracture aperture is maximum,

and thus fluid transmissivity is implemented. In fact the transmissivity (T) controls the fluid flow along a surface, and this strictly depends on the fracture aperture (a) following the equation (Caine and Forster, 1999):

$$T = \frac{a^3}{12} \bullet \frac{\rho g}{\mu}$$

where a is the fracture aperture, ρ is the fluid density, g is the acceleration due to gravity and μ is the fluid viscosity.

In this view, in order to obtain better results during geothermal exploitation, it is arguable that boreholes could be realised following an oblique trajectory (Fig. 19). Additionally, drilling could be realised from the hangingwall block in the direction of the fault plane, with an angle of about 45° with respect to the fault trace, in plane view. This may represent the better geometric condition assuming: (a) most vertical fractures can be intercepted; (b) boreholes intercept most fracture surfaces in perpendicular modality. In addition, it should be advised to perforate down to the fault core, in order to reach the footwall damage zone where most intense hydrothermal circulation can be expected.

Acknowledgements

Suggestions from D. Liotta helped me to prepare this paper. I am very grateful to Marco Bonini and Eric Nelson for their criticism and very constructive comments which improved the manuscript. Suggestions of the Editor, Thomas Blenkinsop, are also much appreciated. Thanks to S. Jones for the English revision. B. Terrosi helped me to realise the digital version of the Figs. 4 and 18. This research was funded by PAR2005 University of Siena research grants (coord. Antonio Lazzarotto).

References

Agosta, F., Aydin, A., 2006. Architecture and deformation mechanism of a basin-bounding normal fault in Mesozoic platform carbonates, central Italy. Journal of Structural Geology 28, 1445–1467.

Antonellini, M., Aydin, A., 1994. Effect of faulting on fluid flow in porous sandstones: petrophysical properties. AAPG Bullettin 78, 355–377.

Antonellini, M., Aydin, A., 1995. Effect of faulting on fluid flow in porous sandstones: geometry and spatial distribution. AAPG Bullettin 79, 642–671.

Aydin, V., 2000. Fractures, faults and hydrocarbon entrapment, migration, and flow. Marine and Petroleum Geology 17, 797–814.

Baldi, A.M., Marzocchi, A., Menegoli, M., 1992. Nuove individuazioni di giacimenti di anidride carbonica in Toscana. Bollettino Associazione Mineraria Subalpina 29/4, 335–435.

Barazzuoli, P., Costantini, A., Fondi, R., Gandin, A., Ghezzo, C., Lazzarotto, A., Micheluccini, M., Salleolini, M., Salvatorini, L., 1988. I travertini di Rapolano sotto il profilo geologico e geologico tecnico. In il Travertino di Siena. Al.Sa.Ba. grafiche Siena.

Barbier, E., 2002. Geothermal energy and current status: An overview. Renewable and Sustainable Energy Reviews 6, 3–65.

Barton, A.C., Zobach, M.D., Moos, D., 1995. Fluid flow along potentially active faults in crystalline rocks. Geology 23, 683–686.

Batini, F., Brogi, A., Lazzarotto, A., Liotta, D., Pandeli, E., 2003. Geological features of Larderello-Travale and Mt Amiata geothermal areas (southern Tuscany Italy). Episodes 26, 239–244.

Bellani, S., Brogi, A., Lazzarotto, A., Liotta, D., Ranalli, G., 2004. Heat flow deep temperatures and extensional structures in the Larderello Geothermal Field (Italy): constraints on geothermal fluid flow. Journal of Volcanology Gethermal Research 132, 15–29.

Berg, S.S., Skar, T., 2005. Controls on damage zone asymmetry of a normal fault zone: outcrop analyses of a segment of the Moab Fault, SE Utah. Journal of Structural Geology 27, 1803–1822.

Bernoulli, D., Kalin, O., Patacca, E., 1979. A Sunken continental margin of the Mesozoic Tethys: the northestern and central Apennines. Symposium "Sedimentation jurassique W Européaen", A.S.F. Publication Spécial 1, 197–210.

Bertini, G., Cameli, G.M., Costantini, A., Decandia, F.A., Di Filippo, M., Dini, I., Elter, F.M., Lazzarotto, A., Liotta, D., Pandeli, E., Sandrelli, F., Toro, B., 1991. Struttura geologica fra i monti di Campiglia e Rapolano Terme (Toscana meridionale): stato attuale delle conoscenze e problematiche. Studi Geologici Camerti Volume Speciale 1, 155–178.

Billi, A., Valle, A., Brilli, M., Faccenna, C., Funiciello, R., 2007. Fracture-controlled fluid circulation and dissolution weathering in sinkhole-prone carbonate rocks from central Italy. Journal of Structural Geology 29, 385–395.

Blampied, M.L., Lockner, D.A., Byerlee, J.D., 1992. An earthquake mechanism based on rapid sealing of faults. Nature 358, 574–576.

Bonini, M., 1999. Basement-controlled Neogene polypshase cover thrusting and basin devolepment along the Chianti Mountains ridge (Northern Apennines, Italy). Geological Magazine 136, 133–152.

Bonini, M., Sani, F., 2002. Extension and compression in the Northern Apennines (Italy) hinterland: Evidence from the late Miocene-Pliocene Siena-Radicofani Basin and relations with basement structures. Tectonics 22, 1–35.

Bossio, A., Costantini, A., Lazzarotto, A., Liotta, D., Mazzanti, R., Mazzei, R., Salvatorini, G., Sandrelli, F., 1993. Rassegna delle conoscenze sulla stratigrafia del neoautoctono toscano. Memorie della Società Geologica Italiana 49, 17–98.

Brogi, A., 2002. Relazione tra strutture distensive neogenico-quaternarie ed i depositi di travertine nell'area di Rapolano Terme (Appennino Settentrionale). Atti Ticinensi di Scienze della Terra 43, 41–54.

Brogi, A., 2004. Faults linkage, damage rocks and hydrothermal fluid circulation: tectonic interpretation of the Rapolano Terme travertines (southern Tuscany, Italy) in the context of the Northern Apennines Neogene-Quaternary extension. Eclogae Geologicae Helvetiae 97, 307–320.

Brogi, A., Costantini, A., Lazzarotto, A., 2002. Tectonic setting of the Rapolano-Trequanda ridge. Bollettino della Società Geologica Italiana Spec. Vol. 1, 757–768.

Brogi, A., Lazzarotto, A., Liotta, D., Ranalli, G. CROP18 Working Group, 2005a. Crustal structures in the geothermal areas of southern Tuscany (Italy): Insights from the CROP 18 deep seismic reflection lines. Journal of Volcanology Geothermal Research 148, 60–80.

Brogi, A., Lazzarotto, A., Liotta, D. CROP18 Working Group, 2005b. Structural features of southern Tuscany and geological interpretation of the CROP18 Seismic Reflection Survey (Italy). Bollettino della Società Geologica Italiana Spec. Vol., 3, 213–236.

Bruhn, R.L., Yonkee, W.A., Parry, W.T., 1990. Structural and fluid-chemical properties of seismogenic normal faults. Tectonophysics 175, 139–157.

Bruhn, R.L., Parry, W.T., Yonkee, W.A., Thompson, T., 1994. Fracturing and hydrothermal alteration in normal fault zones. Pageoph 142, 609–642.

Byerlee, J.D., 1993. Friction, overpressure and fault normal compression. Geophysical Research Letters 17, 2019–2112.

Caine, S.J., Evans, J.P., Forster, C.B., 1996. Fault zone architecture and permeability structure. Geology 24, 1025–1028.

Caine, S.J., Forster, C.B., 1999. Fault zone architecture and fluid flow: insight from field data and numerical modeling. In: Haneberg, W.C., Mozley, P.S., Moore, J.C., Goodwin, L.B. (Eds.), Faults and Subsurface Fluid Flow in the Shallow Crust. Geophysical Monographs 113, pp. 101–127.

Carosi, R., Frassi, C., Montomoli, C., Pertusati, P.C., 2004. Structural evolution of the Tuscan Nappe in the southeastern sector of the Apuan Alps metamorphic dome (Northern Apennines, Italy). Geological Journal 40, 103–119.

Carmignani, L., Decandia, F.A., Disperati, L., Fantozzi, P.L., Lazzarotto, A., Liotta, D., Meccheri, M., 1994. Tertiary extensional tectonics in Tuscany (Northern Apennines Italy). Tectonophysics 238, 295–315.

Cello, G., 2000. A quantitative structural approach to the study of active fault zones in the Apennines (peninsular Italy). Journal of Geodynamics 29, 265–292.

Cello, G., Gambini, R., Mazzoli, S., Read, A., Tondi, E., Zucconi, V., 2000. Fault zone characteristics and scaling properties of the Val d'Agri Fault System (southern Apennines, Italy). Journal of Geodynamics 29, 293–307.

Cello, G., Invernizzi, C., Mazzoli, S., Tondi, E., 2001a. Fault properties and fluid flow patterns from Quaternari faults in the Apennines, Italy. Tectonophysics 336, 63–78.

Cello, G., Tondi, E., Micarelli, L., Invernizzi, C., 2001b. Fault zone fabrics and geofluid properties as indicators of rock deformation modes. Journal of Geodynamics 32, 543–565.

Chan, M.A., Parry, W.T., Bowman, J.R., 2000. Diagenetic hematite and manganese oxides and fault-related fluid flow in Jurassic sandstones, southeastern Utah. AAPG Bullettin 84, 1281–1310.

Chester, F.M., Logan, J.M., 1986. Implications for mechanical properties of brittle faults from observations of the Punchbowl fault zone, California. Pure and Applied Geophysics 124, 79–106.

Chester, F.M., Evans, J.P., Biegel, R.L., 1993. Internal structure and weakening mechanism of the S.Andreas Fault. Journal of Geophysical Research 98, 771–786.

Costantini, A., Lazzarotto, A., Sandrelli, F., 1982. Conoscenze geologico strutturali. In: Il Graben di Siena. CNR PFE RF9, 11–32.

Decandia, F.A., Lazzarotto, A., 1972. Ritrovamento di macroforaminiferi oligocenici nella parte inferiore del Macigno del Chianti in località Farnetella (Siena). Bollettino della Società Geologica Italiana 91, 511–521.

Della Vedova, B., Bellani, S., Pellis, G., Squarci, P., 2001. Deep temperatures and surface heat flow distribution. In: Vai, G.B., Martini, I.P. (Eds.), Anatomy of an Orogen the Apennines and Adjacent Mediterranean Basins. Kluwer Academic Publishers.

Dockrill, B., 2005. Understanding leakage from a fault-sealed CO2 reservoir in east-central Utah: a natural analogue applicable CO2 storage. Unpublished PhD thesis. University of Dublin, Department of Geology, Trinity College. 2005.

Elter, F.M., Sandrelli, F., 1995. Inquadramento strutturale dei Monti del Chianti. Bollettino della Società Geologica Italiana 14, 537–547.

Evans, J.P., Chester, F.M., 1995. Fluid-rock interaction in faults of the S.Andreas system: inferences from San Gabriel fault rock geochemistry and microstructures. Journal of Geophysical Research 100, 13007–13020.

Evans, J.P., Forster, C.B., Goddard, J.V., 1997. Permeability of fault-related rocks, and implications for hydraulic structure of fault zones. Journal of Structural Geology 19, 1393–1404.

Flodin, E., Aydin, A., 2004. Faults with asymmetric damage zones in sandstone, Valley of Fire State Park, southern Nevada. Journal of Structural Geology 26, 983–988.

Gandin, A., 1982. Considerazioni stratigrafico-paleogeografiche. In: Il Graben di Siena. CNR PFE RF9, 34–36.

Gandin, A., Sandrelli, F., 1992. Caratteristiche sedimentologiche dei corpi sabbiosi intercalate nelle argille plioceniche del Bacino di Siena. Giornale di Geologia 54, 55–56.

Guo, L., Riding, R., 1992. Aragonite laminea in hot water crusts, Rapolano Terme, Italy. Sedimentology 39, 1067–1079.

Guo, L., Riding, R., 1994. Origin and diagenesis of Quaternary travertine shrub fabric, Rapolano Terme, central Italy. Sedimentology 41, 499–520.

Guo, L., Riding, R., 1996. Hot-spring travertine facies and sequence, Late pleistocene, Rapolano Terme, Italy. Sedimentology 45, 163–180.

Jourde, H., Flodin, E.A., Aydin, A., Durlofski, L.J., Wen, X.H., 2002. Computing permeability of fault zones in eolian sandstone from outcrop measurement. AAPG Bulletin 86, 1187–1200.

Kalin, O., Patacca, E., Renz, O., 1979. Jurassic pelagic deposits from Southeastern Tuscany; aspects of sedimentation and new biostratigraphic data. Eclogae Geologicae Helvetiae 72, 715–762.

Kim, Y.S., Peacock, D.C.P., Sanderson, D.J., 2004. Fault damage zones. Journal of Structural Geology 26, 503–517.

Labaume, P., Carrio-Schaffhauser, E., Gamond, J.F., Renard, F., 2004. Deformation mechanism and fluid-driven mass transfers in the recent fault zones of the Corinth Rift (Greece). Comptes Rendus Geoscience 336, 375–383.

Lazzarotto, A., 1973. Caratteri strutturali dei nuclei mesozoici di Montalceto, Trequanda e Piazza di Siena (Prov. di Siena). Atti Società Toscana di Scienze Naturali Memorie Serie A 79, 251–266.

Lazzarotto, A., Sandrelli, F., 1977. Stratigrafia e assetto tettonico delle formazioni neogeniche del Bacino del Casino (Siena). Bollettino della Società Geologica Italiana 96, 713–722.

Liotta, D., 1994. Structural features of the Radicofani basin along the Piancastagnaio (Mt. Amiata)—S.Casciano dei Bagni (Mt. Cetona) cross section. Memorie della Società Geologica Italiana 48, 401–408.

Liotta, D., 1996. Analisi del settore centro-meridionale del bacino pliocenico di Radicofani (Toscana meridionale). Bollettino della Società Geologica Italiana 115, 115–143.

Liotta, D., Salvatorini, G., 1994. Evoluzione sedimentaria e tettonica della parte centro-meridionale del bacino pliocenico di Radicofani. Studi Geologici Camerti Vol. Spec. 1994/1, 65–77.

Liotta, D., Cernobori, L., Nicolich, R., 1998. Restricted rifting and its coexistence with compressional structures: results from the Crop03 traverse (Northern Apennines Italy). Terra Nova 10, 16–20.

Losacco, U., 1952. La struttura del territorio di Rapolano e Lucignano (Siena e Arezzo). Bollettino della Società Geologica Italiana 70, 402–434.

Losacco, U., Del Giudice, D., 1958. Stratigrafia e tettonica degli affioramenti mesozoici posti fra le colline di Rapolano ed il Monte Cetona (Siena). Bollettino della Società Geologica Italiana 77, 1–32.

Martini, I.P., Sagri, M., 1993. Tecto-sedimentary characteristics of the late Miocene-Quaternary extensional basins of the Northern Apennines, Italy. Earth Science Reviews 34, 197–233.

Micarelli, L., Benedicto, A., Wibberley, C.A.J., 2006. Structural evolution and permeability of normal fault zones in highly porous carbonate rocks. Journal of Structural Geology 28, 1214–1227.

Minissale, A., Vaselli, O., Tassi, F., Magro, G., Grechi, G.P., 2002. Fluid mixing in carbonate acquifers near Rapolano (central Italy): chemical and isotopic constraints. Applied Geochemistry 17, 1329–1342.

Mongelli, F., Zito, G., 1991. Flusso di calore nella Regione Toscana. Studi Geologici Camerti Vol. Spec. 1, 91–98.

Mongelli, F., Grassi, S., Perusini, P., Squarci, P., Taffi, L., 1982. Misure di flusso di calore (risulati preliminari). In: Graben di Siena. CNF-PFE-RF9, pp. 150–162.

Nelson, E.P., Kullman, A.J., Gardner, M.H., 1999. Fault-fracture networks and related fluid flow and sealing, Brushy Canyon Formation, West Texas. In: Fault and subsurface fluid flow in the shallow crust. Geophysical Monograph 113. American Geophysical Union. 69–81.

Parry, W.T., Bruhn, R.L., 1986. Pore fluid and seismogenic characteristics of fault rocks at depth on the Wasatch Fault, Utah. Journal Geophysical Research 91, 730–744.

Parry, W.T., Wilson, P.N., Bruhn, R.L., 1988. Pore fluid chemistry and chemical reactions on the wasatch normal fault, Utah. Geochimica et Cosmochimica Acta 52, 2053–2063.

Parry, W.T., Hedderly-Smith, D., Bruhn, R.L., 1991. Fluid inclusions and hydrothermal alteration on the Dixie Valley Fault, Nevada. Journal of Geophysical Research 96, 19733–19748.

Parry, W.T., Chan, M.A., Beitler, B., 2004. Chemical bleaching indicates episodes of fluid flow in deformation bands in sanstone. AAPG Bulletin 88, 175–191.

Passerini, P., 1964. Il Monte Cetona (Provincia di Siena). Bollettino Società Geological Italiana 83, 219–238.

Peacock, D.C.P., 2001. The temporal relationship between joints and faults. Journal of Structural Geology 23, 329–341.

Peacock, D.C.P., 2002. Propagation, interaction and linkage in normal fault systems. Earth-Science Reviews 58, 121–142.

Peacock, D.C.P., Knipe, R.J., Sanderson, D.J., 2000. Glossary of normal faults. Journal of Structural Geology 22, 291–305.

Rowland, J.V., Sibson, R.H., 2004. Structural controls on hydrothermal flow in a segmented rift system, Taupo Volcanic Zone, New Zealand. Geofluids 4, 259–283.

Sibson, R.H., 1977. Fault rocks and fault mechanism. Journal of the Geological Society London 133, 191–213.

Sibson, R.H., 1992. Implications of fault-valve behaviour for rupture nucleation and recurrence. Tectonophysics 211, 283–293.

Sibson, R.H., 1996. Structural permeability on fluid-driven fault-fracture meshes. Journal of Structural Geology 18, 1031–1042.

Storti, F., Billi, A., Salvini, F., 2003. Particle size distribution in natural carbonate fault rocks: insights for non-self similar cataclasis. Earth and Planetary Science Letters 206, 173–186.

Tchalenko, J.S., 1970. Similarities between shear zones of different magnitudes. Bulletin of the Geological Society of America 81, 1625–1640.

Wibberley, C.A.J., Shimamoto, T., 2003. Internal structure and permeability of major strike-slip fault zones: the Median Tectonic Line in Mie Prefecture, southwest Japan. Journal of Structural Geology 25, 59–78.

Zhang, X., Sanderson, D.J., 1996. Numerical modelling of the effects of fault slip on fluid flow around extensional faults. Journal of Structural Geology 95, 109–119.